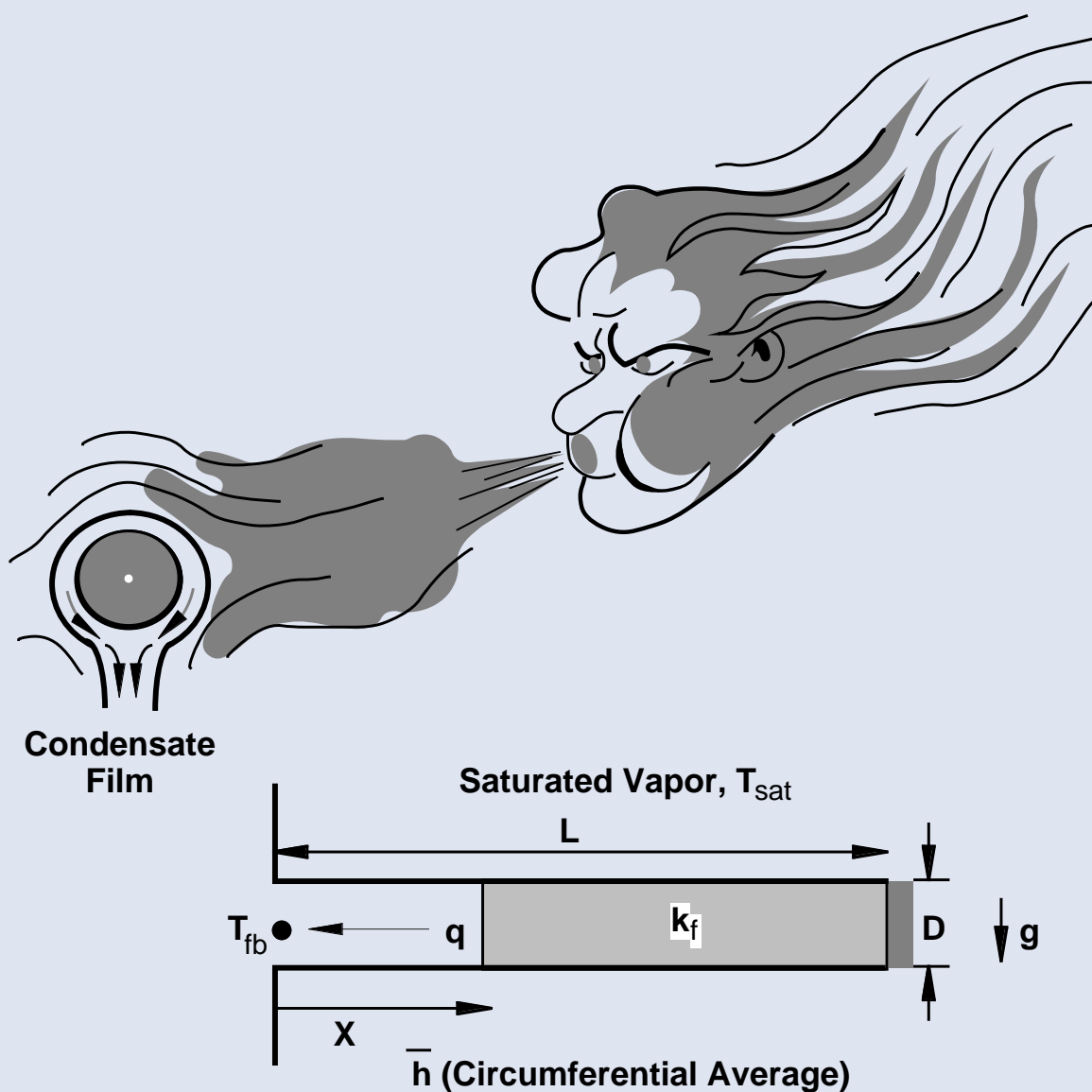# Effect of Condensation on Performance and Design of Extended Surfaces

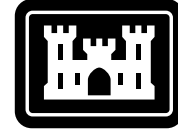Virgil J. Lunardini and Abdul Aziz

November 1995

Condensate Film

Saturated Vapor, T_{sat}

T_{fb} ← q

k_f

D

g

X

$\overline{h}$ (Circumferential Average)

Abstract

Heat transfer surfaces operating in cold regions often involve condensation. The analytical and experimental progress made in understanding the process of condensation on extended surfaces (fins) is reviewed in detail. The review covers condensation of pure vapor as well as dehumidification of air. The analytical models discussed range from simple Nusselt-type analysis to the three-dimensional conjugate approach, in which the conservation equations for the condensate film are tightly coupled to conduction in the fin. A separate section discusses the topic of dehumidification of air on finned cooling coils. Other topics reviewed include condensation on horizontal integral-fin tubes, convective condensation in internally finned tubes, and condensation in micro-fin tubes. Although condensation on horizontal integral-fin tubes appears to be well understood, our understanding of convective condensation in internally finned tubes, particularly the micro-fin tubes, is very limited. Furthermore, there exists no established methodology for designing extended surfaces for condensation applications. This report contains several examples illustrating the theoretical results that provide some insight into the design process.

CRREL Report 95-20

**US Army Corps
of Engineers**
Cold Regions Research &
Engineering Laboratory

Effect of Condensation on Performance and Design of Extended Surfaces

Virgil J. Lunardini and Abdul Aziz   November 1995

PREFACE

The contents of this report are not to be used for advertising or promotional purposes. Citation of brand names does not constitute an official endorsement or approval of the use of such commercial products.

NOMENCLATURE

a	slope of saturation curve or a constant
A	heat transfer area or a constant
b	slope of enthalpy–temperature curve or base distance
B	a constant
Bi	Biot number
c	a constant
c_p	specific heat
C_a	Ackerman correction factor
C_f	interface enhancement factor
d	tube diameter
D	pin fin diameter
D_h	hydraulic diameter
e	fin height
f	stream function
$F, F_1, ... F_4$	parameters
g	acceleration due to gravity or dimensionless temperature
G	mass flux (velocity)
h	local heat transfer coefficient
$\bar{h}$	average heat transfer coefficient
h_{fg}	latent heat of vaporization
h_m	mass transfer coefficient
$\bar{h}_N$	average heat transfer coefficient over N tube rows
H	fin depth
k	thermal conductivity
L	fin length
L_f	average fin height over the diameter d_o
m	exponent or fin parameter
m_1	a constant defined by eq 87
$\dot{m}$	condensate mass flow rate
n	exponent or number of fins
N	number of tubes in a column or fin parameter
N^*	wet fin parameter
p	pitch
P	total pressure
Pr_ℓ	Prandtl number for liquid phase
P_s, T_r	saturation pressure at temperature T_r
P_{va}	partial pressure of water vapor at temperature T_a
q	heat transfer to the base of the fin
q''	heat flux
R	dimensionless radial coordinate or the ratio of sensible to total heat flux

Re_ℓ	condensate Reynolds number
R_v	gas constant for water vapor
s	gap between fins
s_m	maximum length of the condensate interface
T	temperature
U_a	airstream velocity
w	fin thickness
w_t	weight of the tube
w_{tp}	weight of the plain tube
x	axial distance or vapor quality
X	dimensionless axial distance
z	transverse coordinate
Z	dimensionless transverse coordinate

Greek Symbols

α	helix angle
β	condensate flooding angle or fin included angle
Δ	dimensionless film thickness
Δ^*	dimensionless parameter Δ^4/Z
δ	condensate film thickness
η	total surface efficiency
η_f	fin efficiency
θ	dimensionless temperature
θ_m	rotation angle from fin tip to base
μ	absolute viscosity
ν	kinematic viscosity
ξ	similarity variable or interface shape parameter
ρ	density
σ	surface tension
ϕ	relative humidity
ψ	a parameter equal to Δ^4
ω_s	specific humidity of saturated air

Subscripts

a	ambient or air
b	base
bs	saturated at base temperature
c	classical
cr	critical
d	dry
f	fin
fb	fin base
ft	fin tip
h	horizontal or hydraulic
i	condensate-air interface
ℓ	liquid phase
o	outside

p	plain
r	reference or fin root
s	sensible or saturated air
sat	saturated
t	total
v	vapor phase
w	wet
ws	sensible for wet fin
wt	total for wet fin
∞	freestream or ambient

CONTENTS

ILLUSTRATIONS

TABLES

Effect of Condensation on Performance and Design of Extended Surfaces

VIRGIL J. LUNARDINI AND ABDUL AZIZ

INTRODUCTION

Extended surfaces or fins have been traditionally employed to reduce the convective resistance associated with low values of the heat transfer coefficient h such as those encountered in convection to and from gases. In condensation, the typical values of h are high and the need for and the effectiveness of fins for augmentation may not be immediately apparent. However, in the past 50 years, several engineering situations have been identified where augmenting condensation can be beneficial. Consider, for example, the condensation of organic vapors where the poor thermophysical properties result in comparatively low values of h and consequently offer room for enhancement. Even with fluids having favorable thermophysical properties, the condensing side resistance may be significant and warrant reduction, especially if the cold side is augmented. The widespread use of integral fin tubes in surface condensers for the refrigeration and so-called process industries clearly demonstrates the usefulness of fins for enhancing condensation. The use of finned tubes in the cold regions of the world will almost always occur with condensation and the effects of the condensed liquid must be carefully examined.

Vapor on a surface condenses if the temperature of the surface is kept below the vapor saturation temperature. Although four basic mechanisms (homogeneous, direct contact, drop, and film) occur, most condensers are designed to operate under the film condensation mode. The process is characterized by the formation of a thin film of liquid that drains under the action of gravity or surface tension or both. The presence of a film creates a barrier between the vapor and the cooled surface and thus retards the condensation process. If condensation is to be enhanced, the film thickness must be reduced. This reduction can be achieved by using, among other methods, finned surfaces instead of plain surfaces.

The purpose of this report is to serve as a comprehensive review of the published literature on condensation on extended surfaces. The authors hope that the review will be useful to researchers and practicing engineers alike. The report contains several examples that serve to demonstrate the applicability of the material to engineering analysis and design.

To facilitate a systematic presentation, the report has been organized as follows. First, the theory of film condensation on extended surfaces is introduced. The theory utilizes the well-known Nusselt model for the heat transfer coefficient to analyze condensation on three fin configurations: horizontal cylindrical (pin) fin, vertical cylindrical fin, and vertical rectangular fins. This is followed by a discussion of conjugate conduction–condensa-

tion theory, and includes condensation of pure vapor as well as condensation of humid air. Next, a section is devoted to the design of optimum fins for condensation applications. The concluding part of the report refers briefly to vapor space condensation on horizontal integral fin tubes, convective condensation in internally fined tubes, and condensation in micro-fin tubes.

CONDENSATION ON SINGLE FINS

Nusselt-type models

The main difficulty in the analysis of film condensation on fins is the variability of the heat transfer coefficient, h. Unlike the classical fin analysis *that* assumes h to be constant, h for laminar condensation is a function of the difference between the local fin temperature and the saturation of the condensing vapor. Another difficulty is that the surface (fin) is nonisothermal, whereas the simple Nusselt theory applies to an isothermal surface. Despite these difficulties, it will be shown in the following subsections that a localized application of Nusselt theory can be used at least for preliminary analysis and design.

Horizontal cylindrical (pin) fin

Consider a horizontal cylindrical fin of diameter D, length L, and thermal conductivity k_f as shown in Figure 1. The fin is in contact with a pure saturated, quiescent vapor at temperature T_{sat}. The fin is attached to a cooled surface at fin base temperature T_{fb} ($< T_{sat}$). Thus, the fin provides a cooled surface for the adjoining vapor to condense upon. Under steady-state conditions, the latent heat extracted from the vapor is conducted into the colder base. The condensate film formed on the surface of the fin drips down under the action of gravity.
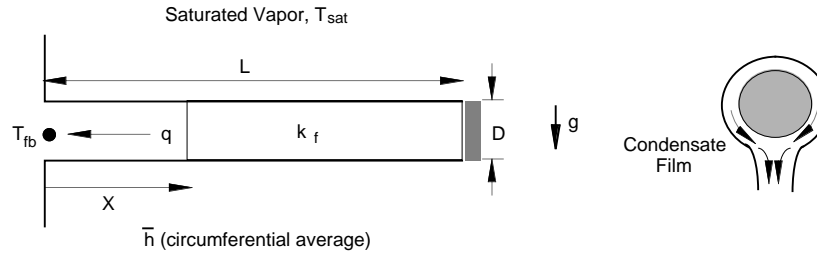
Figure 1. Condensation on a horizontal pin fin.

Let $\bar{h}$ be the circumferentially averaged condensation heat transfer coefficient at any axial location on the fin. Since the values of $\bar{h}$ are usually large, high values of the Biot number $Bi = hD/2k$ occur which, in turn, induce two-dimensional thermal effects in the fin. We ignore this fact to avoid further complication, and assume that axial conduction is the dominant mode of heat transfer through the fin. The equations governing the temperature distribution in the fin can be written as

$$\frac{d^2\theta}{dX^2} - \frac{4\bar{h}L^2}{k_f D}\theta = 0 \tag{1}$$

$$X = 0, \theta = 1 \; ; \; X = 1, \; \frac{d\theta}{dX} = 0 \tag{2a,b}$$

where $\theta = (T_{sat} - T_f)/(T_{sat} - T_{fb}), X = x/L$, and the boundary condition (eq 2b) implies an

insulated fin tip. To obtain $\bar{h}$, we apply the Nusselt theory locally and use the well-known expression for laminar condensation on a single, horizontal tube with zero interfacial shear on the condensate film (Webb 1994). Thus, in terms of θ, we write

$$\bar{h} = 0.728\left[g\rho_\ell(\rho_\ell - \rho_v)k_\ell^3 h_{fg} / \mu_\ell(T_{sat} - T_{fb})\theta D\right]^{1/4} \tag{3}$$

where g = acceleration due to gravity
  ρ_ℓ = density of condensate
  ρ_v = density of vapor
  k_ℓ = thermal conductivity of the condensate
  μ_ℓ = absolute viscosity of the condensate
  h_{fg} = latent heat of condensation.

Substituting for $\bar{h}$ from eq 3 in eq 1 gives

$$\frac{d^2\theta}{dX^2} - N\theta^{3/4} = 0 \tag{4}$$

where the number of tubes on a fin is

$$N = 2.912\left[g\rho_\ell(\rho_\ell - \rho_v)k_\ell^3 h_{hg}L^8 / k_f^4\mu_\ell(T_{sat} - T_{fb})D^5\right]^{1/4}. \tag{5}$$

Since an analytical solution of eq 4 subject to boundary conditions (eq 2a,b) is not feasible, a numerical procedure involving the combination of quasi-linearization and superposition (Na 1979) was used to obtain the solution. Figure 2 displays the numerical results for N = 5, 10, 50 and 100. These results match those of Lienhard and Dhir (1974) who used a shooting method to generate the numerical solutions.

Figure 2 provides some insight into fin design. For N = 50 and 100, the last half of the fin does not sustain any condensation because the temperature difference, $T_{sat} - T_f$, is virtually zero. Such a design is a waste of fin material. At low values of N, say N = 5, the entire fin surface is effective in supporting condensation, but then the fin is too short for substantial condensation augmentation. It is therefore reasonable to conclude that for good design, N should be of the order of 10.
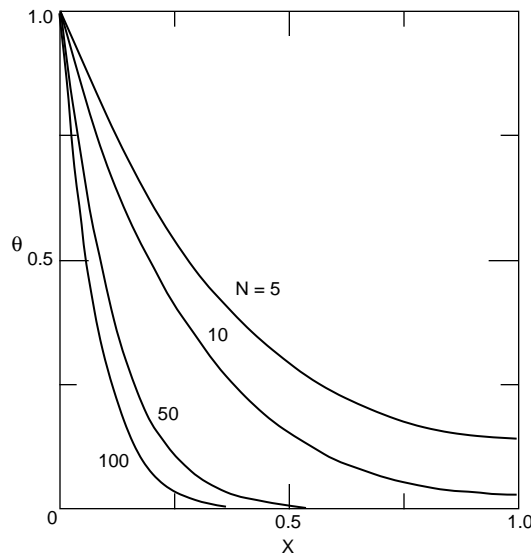
Figure 2. Temperature distributions in a horizontal pin fin with condensation.

3
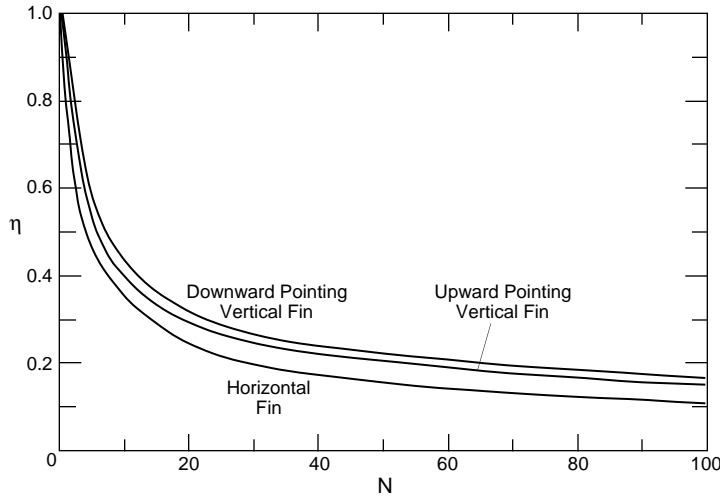
Figure 3. Efficiencies of horizontal and vertical fins with condensation.

The efficiency, η_f, of the fin can be found by computing the heat conducted into the base of the fin and dividing it by $q_{\text{ideal}} = \bar{h}(x=0)\pi DL(T_{\text{sat}} - T_{\text{fb}})$. The resulting expression for η_f is

$$\eta_f = -\frac{1}{N}\frac{d\theta}{dX}\bigg|_{X=0} . \tag{6}$$

The efficiency values calculated from the numerical solution and using eq 6 are plotted in Figure 3. The figure also contains the results for the vertical fins that are discussed in the next section. If $N = 10$ is selected to design the fin, then the corresponding η_f read from Figure 3 is 0.34 or 34%, which is rather low. This low value for η is inevitable if a significant increase in condensation rate is to be realized.

Example 1

Saturated steam at 0.15 bar condenses on a surface at 25°C. It is desired to enhance the rate of condensation by attaching a cylindrical fin made of brass to the primary surface. Suggest some suitable design options.

Solution

For saturated steam at 0.15 bar, the following data apply:

$$T_{\text{sat}} = 54°\text{C}, \ \rho_v = 0.098 \ \text{kg/m}^3 , h_{\text{fg}} = 2373 \ \text{kJ/kg}.$$

Evaluating the properties of condensate at a mean temperature of $(54 + 25)/2 = 39.5°\text{C}$, the following values for properties result:

$$\rho_\ell = 992 \ \text{kg/m}^3, \ \mu_\ell = 663 \times 10^{-6} \ \text{N s/m}^2 , \ k_\ell = 0.631 \ \text{W/m K}.$$

The thermal conductivity of brass is taken as $k_f = 61$ W/m K.

For good design, take $N = 10$. Using eq 5, a relationship between length L and diameter D can be established as follows:

$$\frac{L}{D^{5/8}} = \left(\frac{N}{2.912}\right)^{1/2}\left[\frac{g\rho_\ell(\rho_\ell - \rho_v)k_\ell^3 h_{\text{fg}}L^8}{k_f^4\mu_\ell(T_{\text{sat}} - T_{\text{fb}})}\right]^{1/8} = 0.2244 \ \text{m}^{3/8}.$$
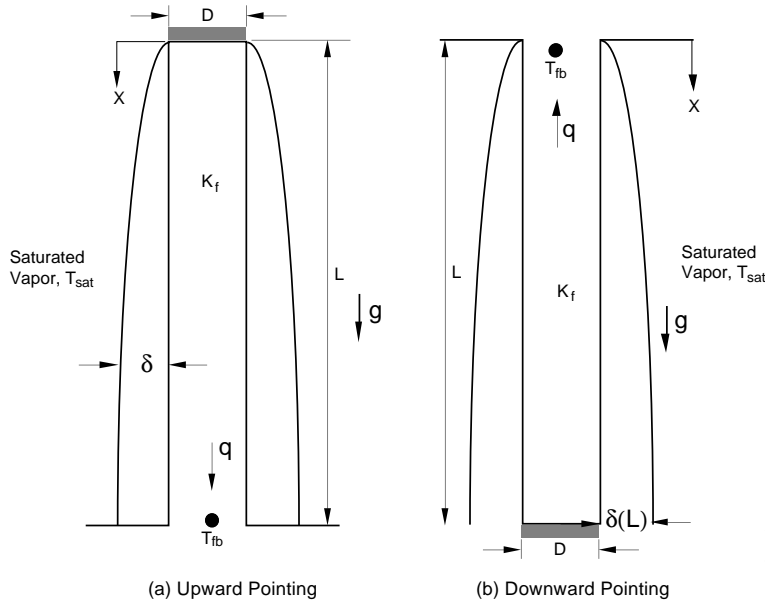
Figure 4. Pin fin in upward and downward vertical orientations.

(a) Upward Pointing   (b) Downward Pointing

Selecting a number of values for *D*, the corresponding values of *L* can be found. The results are summarized below:

D (mm)	*L* (mm)
5	8.18
7.5	10.54
10	12.60
12.5	14.51
15	16.26

Vertical cylindrical (pin) fin

Figure 4 shows a cylindrical fin in two vertical orientations—upward and downward. For the upward pointing fin, the distance x is measured from the tip, while for the downward pointing fin, the same is measured from the base. The essential difference between the horizontal and vertical fins is that for the former, the surface was isothermal along the direction (circumferential) of condensate flow, while in the latter, the temperature decreases for upward configuration or increases for downward configuration along the condensate flow direction. Thus the original Nusselt's theory, which assumes isothermal conditions along the condensate flow direction, is not directly applicable for the vertical fins of Figure 4. However, Lienhard and Dhir (1974) have shown that the Nusselt's theory, if appropriately modified to account for a nonisothermal surface, gives results that are close to the predictions of the full boundary layer equations. For a nonisothermal flat vertical surface, the modified Nusselt's theory gives the following expression for the value of (circumferential average) at any location x from the leading edge:

$$\bar{h} = 0.7071 \left[\frac{g \rho_\ell (\rho_\ell - \rho_v) k_\ell^3 h_{fg}}{\mu_\ell \int_0^x (T_{sat} - T_f) dx} \right]^{1/4}. \tag{7}$$

Equation 7 applies to a cylindrical surface if the curvature effects are small, that is, $\delta(L) \ll 1/2 D$. Using the definitions of θ and X from *Horizontal Cylindrical Fin*, eq 7 can be

recast as follows

$$\bar{h} = 0.7071 \left[\frac{g \rho_\ell (\rho_\ell - \rho_v) k_\ell^3 h_{fg}}{\mu_\ell L (T_{sat} - T_{fb}) \int_0^X \theta \, dX} \right]^{1/4} .$$ (8)

Substituting $\bar{h}$ from eq 8 in eq 1, the following integro-differential equation for θ is obtained:

$$\frac{d^2\theta}{dX^2} - N\theta \left[\int_0^X \theta \, dX \right]^{-1/4} = 0$$ (9)

where

$$N = 2.8284 \left[\frac{g \rho_\ell (\rho_\ell - \rho_v) k_\ell^3 h_{fg} L^7}{\mu_\ell k_f^4 D^4} \right]^{1/4} .$$ (10)

Equation 9 applies to both configurations of Figure 4, but the boundary conditions are different. For the upward pointing fin, these are

$$X = 0, \quad \frac{d\theta}{dX} = 0; \quad X = 1, \quad \theta = 1 .$$ (11a,b)

For the downward pointing fin, the boundary conditions are

$$X = 0, \quad \theta = 1; \quad X = 1, \quad \frac{d\theta}{dX} = 0 .$$ (12a,b)

Numerical solutions of eq 9 subject to boundary conditions (eq 11a,b or 12a,b) have been reported by Lienhard and Dhir (1974). Figure 5 is an adaptation of their results. A close examination of the left and the right portions of Figure 5 reveals that the tempera-
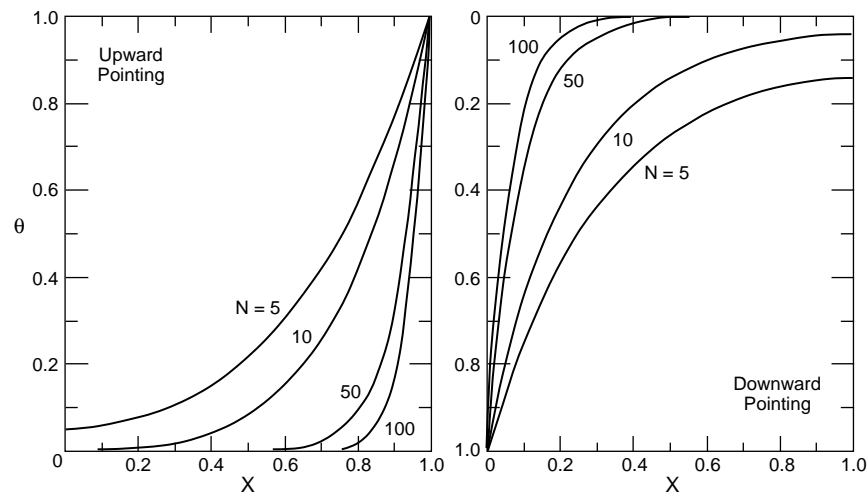

Figure 5. Temperature distributions in vertical pin fins. Adapted from Lienhard and Dhir (1974).

ture profiles for the two orientations are slightly different. As in the case of the horizontal fin, a good design value of N is on the order of 10.

Equation 6 for the fin efficiency also applies to the vertical fins. The results for the efficiency of vertical fins are shown in Figure 3 to allow a comparison with the horizontal fin. Figure 3 shows that vertical fins are more efficient than horizontal fins and, of the two vertical arrangements in Figure 4, the downward pointing fin has a higher efficiency than the upward pointing fin.

Vertical rectangular fin

The results of the foregoing section are also applicable to a vertical rectangular fin if the definition of N is modified appropriately to represent the rectangular geometry.

Conjugate models

In the conjugate models, the heat conduction equation for the fin and the condensate boundary layer equations are solved simultaneously. In the simple model, which has been used by Nader (1978), Burmeister (1982) and Acharya et al. (1986), both the T_f and δ are allowed to vary along the condensate flow direction only; that is, a one-dimensional fin model is used with a two-dimensional condensate film. The improved model proposed by Patankar and Sparrow (1979) considers a two-dimensional fin with a three-dimensional condensate layer.

Simple conjugate model

Consider a vertical fin of rectangular profile as shown in Figure 6. The fin has length L, thickness w, and thermal conductivity k_f. Both faces of the fin are exposed to a saturated vapor at temperature, $T_{sat} > T_{fb}$. The boundary conditions for the fin are those of constant base temperature $T_{fb} < T_{sat}$ and no heat flow through the tip. To establish the conservation equations, consider a slice (fin and two films) of thickness dx. Equating the heat conducted through the two condensate films to the net heat conducted through the fin slice gives

$$\frac{d^2 T_f}{dx^2} = \frac{-2k_\ell \left(T_{sat} - T_f\right)}{kw\delta} \tag{13}$$

where w is fin thickness and δ the condensate film thickness at x. In deriving eq 13, the temperature distribution through the condensate film has been assumed to be linear. The film thickness δ can be related to the local temperature difference, $T_f - T_{sat}$, through the application of the momentum equation, giving

$$\frac{d(\delta^4)}{dx} = \frac{4\mu_\ell k_\ell \left(T_{sat} - T_f\right)}{g\rho_\ell(\rho_\ell - \rho_v)h_{fg}} . \tag{14}$$

It is convenient to introduce the following dimensionless quantities:

$$\theta = \left(T_{sat} - T_f\right)/\left(T_{sat} - T_{fb}\right), X = x/L, \Delta = \delta/L \tag{15}$$

$$F_1 = \frac{g\rho_\ell \left(\rho_\ell - \rho_v\right)h_{fg}L^3}{\mu_\ell k_\ell \left(T_{sat} - T_{fb}\right)} \quad , \quad F_2 = \frac{k_f w}{2k_\ell L}$$

into eq 13 and 14 to give

$$\frac{d^2\theta}{dX^2} = \frac{\theta}{\Delta F_2} \tag{16}$$

$$\frac{d(\Delta^4)}{dX} = \frac{4\theta}{F_1} \quad . \tag{17}$$

The boundary conditions for eq 16 and 17 are

$$X = 0, \quad \Delta = 0, \frac{d\theta}{dX} = 0; \quad X = 1, \theta = 1 \quad . \tag{18a,b}$$

Nader (1974) obtained a numerical solution of eq 16–18, while Burmeister (1982) developed an approximate analytical solution of the same equations. Acharya et al. (1986) solved the dimensional equations (13 and 14) using an iterative numerical scheme. They also extended their computations to six other fin shapes (triangular, trapezoidal, convex parabolic, concave parabolic, cylindrical, and conical) and developed simple correlations for the fin efficiency.

Nader's solution
Nader (1974) introduced a new variable $\psi = \Delta^4$ which enabled him to transform eq 16 and 17 into two, coupled first-order differential equations. These are

$$\frac{d\psi}{dX} = \frac{4\theta}{F_1} \tag{19}$$

$$\frac{d\theta}{dX} = \frac{F_1}{3F_2} \psi^{3/4} \tag{20}$$

subject to

$$X = 0, \psi = 0; \qquad X = 1, \theta = 1. \tag{21a.b}$$

Solving the foregoing equations numerically, Nader obtained the values of tip temperature, $\theta(0)$ for a range of values of F_1 and F_2. These values are recorded in Table 1.

The rate of heat conduction into the base of the fin, q can be obtained as

Table 1. Tip temperatures for a vertical rectangular fin.

F_1/F_2	10^4	10^3	10^2	10
10^7	0.9970	0.9703	0.7460	0.0875
10^8	0.9947	0.9479	0.6011	0.0169
10^9	0.9905	0.9096	0.4182	0.0007
10^{10}	0.9832	0.8461	0.2307	—
10^{11}	0.9703	0.7460	0.0875	—
10^{12}	0.9479	0.6011	0.0169	—
10^{13}	0.9096	0.4183	0.0070	—
10^{14}	0.8461	0.2307	—	—
10^{15}	0.7460	0.0875	—	—
10^{16}	0.6011	0.0169	—	—
10^{17}	0.4183	—	—	—

$$q = 2k_\ell\left(T_{\text{sat}} - T_{\text{fb}}\right)F_2\left.\frac{d\theta}{dX}\right|_{X=1} . \tag{22}$$

The ideal heat transfer, q_{ideal}, occurs when the entire fin is at temperature T_{fb} and is given by

$$q_{\text{ideal}} = 2\bar{h}L\left(T_{\text{sat}} - T_{\text{fb}}\right) \tag{23}$$

where $\bar{h}$ is the average heat transfer coefficient for condensation on an isothermal vertical surface. The expression for $\bar{h}$ based on Nusselt's theory is

$$\bar{h} = 0.943\left[\frac{g\rho_\ell\left(\rho_\ell - \rho_v\right)k_\ell^3 h_{\text{fg}}}{\mu_\ell\left(T_{\text{sat}} - T_{fb}\right)L}\right]^{1/4} \tag{24}$$

which in terms of F_1 becomes

$$\bar{h} = 0.943\frac{k_\ell}{L}F_1^{1/4} . \tag{25}$$

Combining eq 23 and 25 and noting that $\eta = q/q_{\text{ideal}}$, we have

$$\eta_{\text{f}} = 1.0604\frac{F_2}{F_1^{1/4}}\left.\frac{d\theta}{dX}\right|_{X=1} . \tag{26}$$

The efficiency values obtained from eq 26 appear in Table 2.

The film thickness δ at $x = L$, the condensate flow rate $\dot{m}$ at $x = L$, and the heat conducted into the base of the fin q, can all be expressed in terms of F_1 and η_{f} giving

$$\delta(L) = 1.412L\eta_{\text{f}}^{1/3}F_1^{-1/4} \tag{27}$$

$$\dot{m}(L) = 1.8856k_\ell\left(T_{\text{sat}} - T_{\text{fb}}\right)\eta_{\text{f}}F_1^{1/4} / h_{\text{fg}} \tag{28}$$

$$q = 1.8856k_\ell\left(T_{\text{sat}} - T_{\text{fb}}\right)\eta_{\text{f}}F_1^{1/4} . \tag{29}$$

Table 2. Condensation efficiency of a rectangular vertical fin.

F_1/F_2	10^4	10^3	10^2	10
10^7	0.9988	0.9857	0.8745	0.4603
10^8	0.9979	0.9747	0.7981	0.3612
10^9	0.9955	0.9563	0.6969	0.2823
10^{10}	0.9919	0.9254	0.5776	—
10^{11}	0.9857	0.8745	0.4603	—
10^{12}	0.9747	0.7989	0.3612	—
10^{13}	0.9562	0.6969	0.2823	—
10^{14}	0.9254	0.5776	—	—
10^{15}	0.8745	0.4603	—	—
10^{16}	0.7989	0.3612	—	—
10^{17}	0.6969	—	—	—

Example 2

Pure saturated steam at 60°C condenses on the outside surface of a 50-mm diameter horizontal tube maintained at a uniform temperature of 34°C. Calculate the rate at which heat is transferred to the tube and the condensate flow rate. To enhance the rate of condensation, the tube is fitted with a vertical fin of rectangular profile. The fin is 2 mm thick and 7.5 mm long, and has a thermal conductivity of 48 W/m K. Calculate the rate at which steam condenses on the two faces of the fin and compare this with the rate of condensation on the fin's base area if the fin is absent.

Solution

For saturated steam at 60°C, we have

$$\rho_v = 0.129 \text{ kg/m}^3, \ h_{fg} = 2358 \text{ kJ/kg} .$$

Evaluating the properties of condensate at a mean temperature of 47°C, we have

$$\rho_\ell = 989.1 \text{ kg/m}^3, \ \mu_\ell = 577 \times 10^{-6} \text{ N s/m}^2, \ k_\ell = 0.640 \text{ W/m K}.$$

The average heat transfer coefficient for laminar film condensation on an isothermal horizontal tube is given by eq 3 with $\theta = 1$ (isothermal):

$$h = 0.728 \left[\frac{g\rho_\ell(\rho_\ell - \rho_v)k_\ell^3 h_{fg}}{\mu_\ell(T_{sat} - T_{fb})D} \right]^{1/4} = 6864 \text{ W/m}^2\text{K} .$$

The rate at which heat is transferred to the tube is given by

$$q = \bar{h}\pi D(T_{sat} - T_{fb}) = 28,033 \text{ W/m}.$$

The condensate flow rate $\dot{m}$ is given by

$$\dot{m} = \frac{q}{h_{fg}} = 1.19 \times 10^{-2} \text{kg/s m} .$$

To evaluate q and $\dot{m}(L)$, we first calculate F_1 and F_2 as follows:

$$F_1 = \frac{g\rho_\ell(\rho_\ell - \rho_v)k_{fg}L^3}{\mu_\ell k_\ell(T_{sat} - T_{fb})} = 9.94 \times 10^8 \cong 10^9$$

$$F_2 = \frac{k_f w}{2k_\ell L} = 10 .$$

For $F_1 = 10^9$ and $F_2 = 10$, Table 2 gives $\eta = 0.2823$. Using eq 28, the condensate flow rate, $\dot{m}(L)$ is

$$\dot{m}(L) = 1.8854 k_\ell(T_{sat} - T_{fb})\eta F_1^{1/4} / h_{fg} = 6.67 \times 10^4 \text{kg/s m}.$$

The condensation rate on the base of the fin in the absence of fin is $(1.19 \times 10^{-2}) (0.002)/(\pi)(0.05) = 1.51 \times 10^{-4}$ kg/s m. Comparing this with the figure of 6.67×10^{-4} kg/s m, the fin is seen to enhance condensation by a factor of 4.4.

Burmeister's solution

Burmeister (1982) combined eq 16 and 17 into a single equation and obtained an approximate analytical solution for it. His solutions for the tip temperature $\theta(0)$, heat transfer rate q, and fin efficiency are

$$\theta(0) = 1/\cosh F \tag{30}$$

$$q = 1.8263 k_\ell \left(T_{\text{sat}} - T_{\text{fb}}\right) \left(F_1 F_2^3\right)^{1/7} \tanh^{6/7} F \tag{31}$$

$$\eta = \left(\frac{\tanh F}{F}\right)^{6/7} \tag{32}$$

where

$$F = 1.038 \left(F_1 F_2^4\right)^{1/8}. \tag{33}$$

The efficiency values predicted by eq 32 are in close agreement with the values given in Table 2.

Archarya et al. solution

Archarya et al. (1986) considered vertical fins (Fig. 6) of seven profile shapes, namely rectangular, triangular, trapezoidal, concave parabolic, convex parabolic, cylindrical and conical. For each geometry, they solved eq 13 and 14 numerically and obtained the results for η. For all seven shapes, the efficiency could be represented by a simple relationship of the form

$$\eta = \eta_c^{0.855} \tag{34}$$

where η_c is the efficiency of the fin calculated from classical one-dimensional fin theory and assuming the heat transfer coefficient to be constant for all shapes, its value being given by eq 24. Expressions for η_c for different shapes can be found in Kern and Kraus (1972).

Improved conjugate model

Kazeminejad (1993) improved the simple conjugate model described by eq 16–18 by including the effect of vapor velocity. As expected, the effect of vapor shear was to reduce the condensate film thickness and hence increase the fin surface temperature. The heat transfer to the fin and its capability to support condensation is considerably enhanced.

Patankar and Sparrow (1979) considered film condensation on a vertical rectangular fin, which is attached to a cooled vertical base at temperature T_{fb} (Fig. 7). The fin has length L, thickness w and depth H, and is made of a material with thermal conductivity k_f. The fin is immersed in a pure saturated vapor at temperature T_{sat} ($> T_{\text{fb}}$).
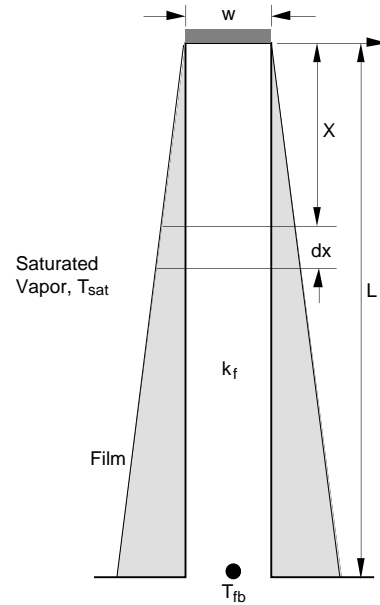

Figure 6. Condensation on a vertical fin of rectangular profile.

11
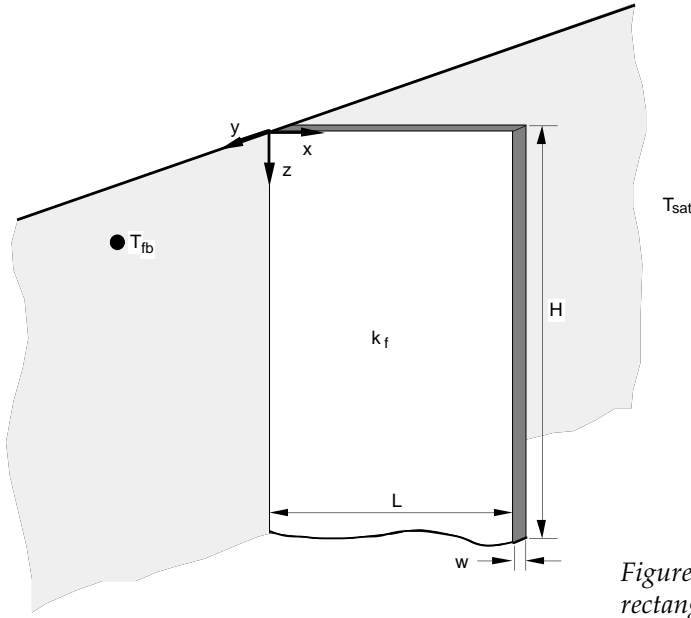
Figure 7. Two-dimensional vertical fin of rectangular profile.

The analysis assumes the fin temperature T_f and the film thickness δ to be functions of x and z; that is, $T_f = T_f(x,z)$ and $\delta = \delta(x,z)$. These assumptions can be justified as follows. As the condensate film flows downward along the fin, more condensate is added to it, and its thickness increases along z to accommodate the increased flow rate. Along the x direction, the temperature differential, $T_{sat} - T_f$, decreases from the base ($x = 0$) of the fin to the tip ($x = L$) of the fin. Consequently, δ also decreases along the x direction. Thus the physics of the process dictates that δ is a function of x and z. The effect of the growth of δ with z is to increase the thermal resistance of the film, thereby decreasing the heat conduction into the fin. The decreased heat flow implies that the fin temperature at a given x must decrease along the z direction. Thus the temperature distribution in the fin is also two-dimensional; that is, $T_f = T_f(x,z)$.

Considering a fin element of dimensions dx, dy and w and making an energy balance gives

$$\frac{\partial^2 T_f}{\partial x^2} = \frac{2k_\ell\left(T_f - T_{sat}\right)}{k_f w \delta} \ . \tag{35}$$

Equation 35 assumes that in the fin, conduction in the x direction is dominant, while in the film, conduction in the y direction is dominant. The momentum equation for the z direction takes the form

$$\frac{\partial}{\partial z}\left(\delta^4\right) = \frac{4\mu_\ell k_\ell\left(T_{sat} - T_f\right)}{g\rho_\ell\left(\rho_\ell - \rho_v\right)h_{fg}} \ . \tag{36}$$

Equations 35 and 36 constitute two coupled partial differential equations for $T_f(x,z)$ and $\delta(x,z)$.

For convenience, the following dimensionless quantities are introduced into eq 35 and 36:

$$\theta = \left(T_f - T_{sat}\right)/\left(T_{fb} - T_{sat}\right) \ , \quad X = x/L$$

12

$$Z = \frac{\mu_\ell k_\ell (T_{sat} - T_{fb})}{4g\rho_\ell (\rho_\ell - \rho_v) h_{fg}} \left[\frac{k_f w}{k_\ell L^2} \right]^4 z, \qquad \Delta = \left(\frac{k_f w}{2k_\ell L^2} \right) \delta \tag{37}$$

which then become

$$\frac{\partial^2 \theta}{\partial X^2} = \frac{\theta}{\Delta} \tag{38}$$

$$\frac{\partial (\Delta^4)}{\partial Z} = \theta . \tag{39}$$

The boundary conditions on θ and Δ are

$$X = 0, \theta = 1; X = 1, \frac{\partial \theta}{\partial X} = 0 \tag{40a,b}$$

$$Z = 0 , \ \Delta = 0 . \tag{41}$$

Patankar and Sparrow (1979) sought a similarity solution of eq 38–41 by arguing as follows. The Nusselt's theory on a vertical isothermal shows that the local heat transfer coefficient h_Z is proportional to $Z^{-1/4}$, giving high values for h_Z at small values of Z. The high values of h_Z cause the fin temperature to increase rapidly from T_b at $x = 0$ to T_{sat}, significantly before $x = L$. Thus the behavior of the fin closely approximates that of an infinitely long fin, permitting the condition eq 40b to be replaced by

$$X = \infty , \ \ \theta = 0 . \tag{42}$$

In the limit $Z = 0$, h_Z becomes infinite and the temperature distribution in the fin takes the form of a step increase from T_b to T_{sat}. Mathematically, this means

$$Z = 0 , \ X > 0 , \ \theta = 0 . \tag{43}$$

Examining the behavior of δ, one notes that at small values of Z, δ must diminish quite rapidly with X to reflect the rapid decrease of $T_{sat} - T$ with X. This permits us to write

$$X = \infty , \ \ \Delta = 0 . \tag{44}$$

The behavior of θ and Δ at $Z = 0$ and $X = \infty$ indicates the possibility of a similarity solution.

Similarity solutions
The introduction of a similarity variable ξ as

$$\xi = X / Z^{1/8} \tag{45}$$

with dependent variables

$$\theta^*(\xi) = \theta, \Delta^*(\xi) = \Delta^4 / Z \tag{46}$$

reduces the partial differential eq 38 and 39 to the following ordinary differential equations

$$\frac{d^2\theta^*}{d\xi^2} - \theta^*(\Delta^*)^{-1/4} = 0 \tag{47}$$

$$\frac{d\Delta^*}{d\xi} - 8(\theta^* - \Delta^*)\xi^{-1} = 0 \tag{48}$$

with the boundary conditions

$$\xi = 0, \theta^* = 1; \xi = \infty, \theta^* = \Delta^* = 0. \tag{49a,b}$$

Patankar and Sparrow (1979) observed that an analytical solution of eq 47–49 was not possible, but Wilkins (1980) showed that an analytical solution does exist and can be written as

$$\theta = \theta^* = \begin{cases} \left(1 - \dfrac{\xi}{\sqrt{42}}\right)^7 & , \ 0 \le \xi \le \sqrt{42} \\ 0 & , \ \xi > \sqrt{42} \end{cases} \tag{50}$$

$$\Delta^* = \begin{cases} \left(1 - \dfrac{\xi}{\sqrt{42}}\right)^8 & , \ 0 \le \xi \le \sqrt{42} \\ 0 & , \ \xi > \sqrt{42} \end{cases} \tag{51}$$

Using eq 50, the temperature gradient

$$\left.\frac{\partial \theta}{\partial X}\right|_{X=0}$$

can be found. Integrating

$$\left.\frac{\partial \theta}{\partial X}\right|_{X=0}$$

from $Z = 0$ to $Z = Z$, the heat conducted into the base of the fin over a distance Z can be evaluated. The final result is

$$q(Z) = 4.9371 \left[\frac{g\rho_\ell(\rho_\ell - \rho_v)k_\ell^3 h_{fg} L^7}{\mu_\ell k_f^3 w^3}\right] Z^{7/8} \ . \tag{52}$$

The ideal heat transfer $q_{ideal}(Z)$ can be found by assuming the entire fin to be isothermal at temperature T_b and using $\bar{h}$ from eq 34. This gives

$$q_{ideal}(Z) = 5.333 \left[\frac{g\rho_\ell(\rho_\ell - \rho_v)k_\ell^3 h_{fg} L^7}{\mu_\ell k_f^3 w^3}\right] Z^{3/4} \ . \tag{53}$$

The fin efficiency η expressed as the ratio of $q(Z)/q_{ideal}(Z)$ is found to be

$$\eta = 0.9257 Z^{1/8} \ . \tag{54}$$

14
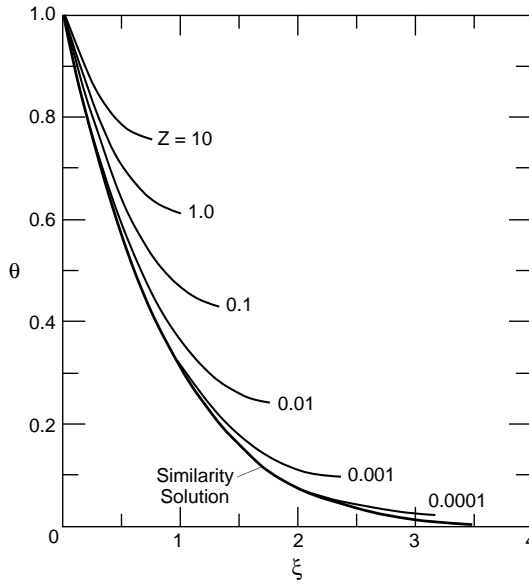
Figure 8. Nonsimilar temperature profiles in a vertical rectangular fin. Adapted from Patankar and Sparrow (1970).
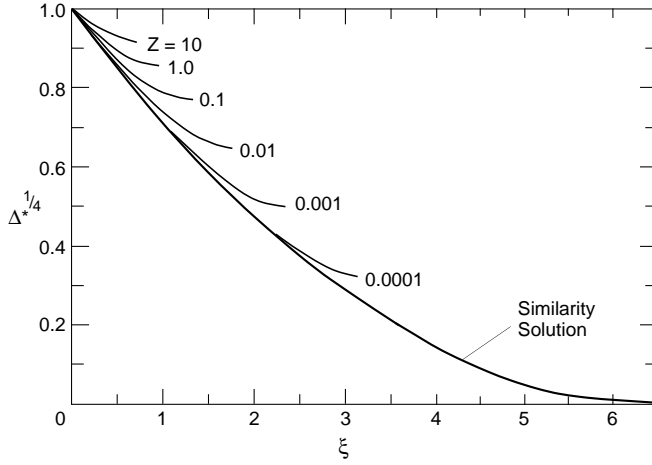
Figure 9. Similar and nonsimilar distributions of condensate film thickness. Adapted from Patankar and Sparrow (1970).

The similarity solutions for θ, Δ^*, and η are shown in Figures 8, 9, and 10, respectively. These figures also show the nonsimilarity solutions that are discussed next.

Nonsimilarity solutions

The applicability of the similarity solutions is limited to those z locations for which the boundary condition eq 42 is justified, that is, locations where the tip temperature is nearly equal to the vapor saturation temperature ($\theta = 0$). For z locations where this condition is not met, eq 38–41 were solved numerically by Patankar and Sparrow (1979). These results appear in Figures 8–10.

Figure 8 shows the temperature profiles at various Z locations. For low values of Z, the temperature distribution in the fin is quite steep as envisioned earlier. As Z increases, the profiles become less and less steep, since larger values of $\theta = \left(T_f - T_{\text{sat}}\right)/\left(T_{\text{fb}} - T_{\text{sat}}\right)$ mean lower values for T (note that $T_b - T_{\text{sat}}$ is negative); one concludes from Figure 8 that the general level of fin temperature decreases as Z increases. This confirms the earlier hypothesis about the dependence of T on Z. Since the nonsimilarity temperature profiles must terminate at $X = 1$, the terminal point on $\xi = X/Z^{1/8}$ scale occurs at lower and lower values of ξ as Z increases. The similarity solution, on the other hand, extends up to $\xi = \sqrt{42} = 6.48$.

15
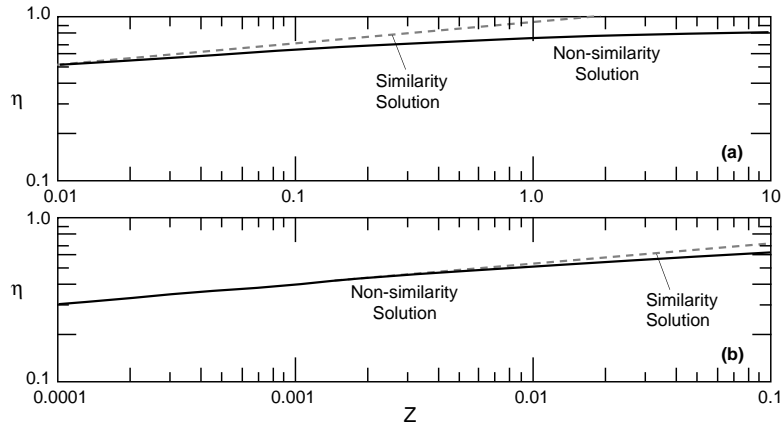
Figure 10. Comparison of similarity and nonsimilarity results for the fin efficiency. Adapted from Patankar and Sparrow (1970).

The condensate film thickness results are shown in Figure 9. For a fixed Z location, the film thickness decreases as x or ξ increases, and this is consistent with the temperature differential $(T_{sat} - T)$ decreasing along X. For small Z, the film is highly nonuniform along the X direction but becomes more and more uniform as Z increases. This clearly shows that the assumption $\delta = \delta(Z)$ employed in previous sections is not strictly valid.

Figure 10 shows the fin efficiency as a function of Z. The lower two curves cover the range of Z from 0.0001 to 0.1, while the upper two curves cover the Z values from 0.01 to 10. Interestingly the similarity and nonsimilarity solutions for η are virtually identical up to $Z = 0.01$. Thus for $Z \leq 0.01$, eq 54 for η and hence eq 52 for $q(Z)$ give accurate predictions. However, this is not true of the similarity results for θ and Δ^*. For example, Figure 8 and 9 shows that for $Z = 0.01$, there is a significant difference between the similarity and the nonsimilarity solutions.

Example 3

A vertical rectangular fin ($k = 400$ W/m K) is attached to a cooled vertical surface (Fig. 7). The fin dimensions are $L = 1.5$ cm, $w = 1.5$ mm, and $H = 25$ cm. The environment surrounding the fin is saturated steam at 50°C. Calculate (i) the rate at which heat is removed by the cooled surface, (ii) the condensation rate supported by the fin, (iii) the fin temperature and the film thickness at $H = 1.5$ cm, $z = 25$ cm.

Solution

The density and heat of vaporization for steam at 50°C are

$$\rho_v = 0.082\,\text{kg}/\text{m}^3 \,, \quad h_{fg} = 2.383 \times 10^6\,\text{J}/\text{kg}.$$

Evaluating the properties of water (condensate) at a mean temperature of $(24 + 50)/2 = 37$°C, we have

$$\rho_\ell = 993\,\text{kg}/\text{m}^3 \,, \mu_\ell = 694 \times 10^{-6}\,\text{N s}/\text{m}^2 \,, k_\ell = 0.628\,\text{W}/\text{m K}.$$

Using the above properties in eq 37, Z can be evaluated:

$$Z = \frac{\mu_\ell k_\ell (T_{sat} - T_{fb})}{4g\rho_\ell(\rho_\ell - \rho_v)h_{fg}}\left[\frac{k_f w}{k_\ell L^2}\right]^4 z = 0.01 \,.$$

16

(i) Since Z is within the limit of applicability of the similarity solution, eq 52 can be used to compute the rate at which heat is removed by the cooled surface:

$$q = 4.9371 \left[\frac{g\rho_\ell(\rho_\ell - \rho_v)k_\ell^3 h_{fg} L^7}{\mu_\ell k^3 W^3} \right] Z^{7/8} = 571\,\text{W} \cdot$$

(ii) The condensate rate supported by the fin is given by

$$\dot{m} = \frac{q}{h_{fg}} = 2.396 \times 10^{-4}\,\text{kg/s} = 0.86\,\text{kg/h} \cdot$$

(iii) Reading the terminal value of θ for the curve marked $Z = 0.01$ in Figure 8, the dimensionless tip temperature is $q_t = 0.25$. Thus

$$\theta_t = \frac{T_{ft} - T_{sat}}{T_{fb} - T_{sat}} = 0.25$$

or $\qquad T_{ft} = 0.25\left(T_{fb} - T_{sat}\right) + T_{sat} = 43.5°\text{C}.$

Similarly, the terminal value of $\Delta^{*1/4}$ for the curve marked $Z = 0.01$ in Figure 9 gives $\Delta^{*1/4} = 0.65$. Using eq 46,

$$\Delta = \Delta^{*1/4}\,(Z)^{1/4} = (0.65)\,(0.01)^{1/4}\,0.2055\ .$$

Invoking the definition of Δ, that is, eq 37, the film thickness δ is given by

$$\delta = 2k_\ell L^2 \Delta / kw = 0.0968\,\text{mm}$$

DEHUMIDIFICATION OF AIR ON FINS

In air conditioning applications, finned cooling coils are often used to cool and dehumidify air. The thermal performance of these coils is not only affected by geometry, materials and psychrometric conditions, but also by the efficiency of the fin. If the fin temperature is lower than the dew point of air passing over the coil, then the moisture is condensed on the fin surface and affects the fin efficiency.

This section considers the performance of fins operating in moist air streams, with moisture condensation occurring on their surface. *Simple Models* discusses simple models in which the classical fin theory for dry fins is modified to take into account the effect of mass transfer. *Conjugate Models* describes two conjugate models for simultaneous heat and mass transfer to a cooling and dehumidifying vertical rectangular fin. Experimental studies of dehumidification in finned coil heat exchangers are covered in *Experimental Studies*. The design of optimum-dimensional rectangular and triangular fins with condensation is covered in *Optimum Fin Design*.

Simple models

Longitudinal fins

McQuiston (1975) considered moisture condensation on a longitudinal fin of rectangular profile having a length L, thickness w, and thermal conductivity k_f. Let h_d be the

average heat transfer coefficient for dry operating conditions. For the moisture condensation situation, McQuiston, neglecting the thermal resistance of the condensate, postulated that the local driving potential for simultaneous heat and mass transfer was the difference between the enthalpy of air adjacent to the fin and that of saturated air at the local fin temperature. By approximating the saturation curve on the psychrometric chart by a straight line over a small range of temperatures, he expressed the slope a as

$$a = (\omega_{s,2} - \omega_{s,1})/(T_2 - T_1) \tag{54}$$

where ω_s is the specific humidity of saturated air. The heat transfer coefficient h_w for wet conditions was expressed in terms of h_d and a as follows:

$$h_w = h_d \left(1 + \frac{a h_{fg}}{c_p} \right) \tag{55}$$

where c_p is the specific heat of moist air at constant pressure.

In an earlier paper, Ware and Hacha (1960) recommended the following expression for h_w:

$$h_w = h_d \, b/c_p \tag{56}$$

where b is the slope of the enthalpy–temperature curve for saturated air.

With h_w specified by either eq 55 or 56, the conventional fin theory can be employed to obtain the efficiency of a wet fin. For boundary conditions of constant base temperature and insulated tip, the fin efficiency can be expressed as

$$\eta_w = \frac{\tanh N^*}{N^*} \tag{57}$$

where $N^* = \left(2h_w / k_f w \right)^{1/2} L$.

Radial fins

Elmahdy and Biggs (1983) considered a radial fin of base radius r_b, tip radius r_t, thickness w, and thermal conductivity k, exposed to a stream of moist air at temperature T_a and with specific humidity ω_a. If the average heat and mass transfer coefficients are h and h_m, respectively, then the differential equation governing the temperature distribution in the fin can be written as

$$\frac{d^2 T_f}{dr^2} + \frac{1}{r} \frac{dT_f}{dr} - \frac{2h}{kw} (T_a - T_f) - \frac{2h_m}{kw} (\omega_a - \omega_{T,s}) h_{fg} = 0 \tag{58}$$

where $\omega_{T,s}$ is the saturated specific humidity of air corresponding to the local fin temperature T_f. Assuming a constant fin base temperature T_{fb} and insulated fin tip, the boundary conditions for eq 58 can be written as

$$r = r_b, \ T_f = T_{fb}; \quad r = r_t, \ \frac{dT_f}{dr} = 0. \tag{59}$$

Next $\omega_{T,s}$ is assumed to be a linear function of temperature T_f, that is,

$$\omega_{T,s} = c + a \, T_f \tag{60}$$

18
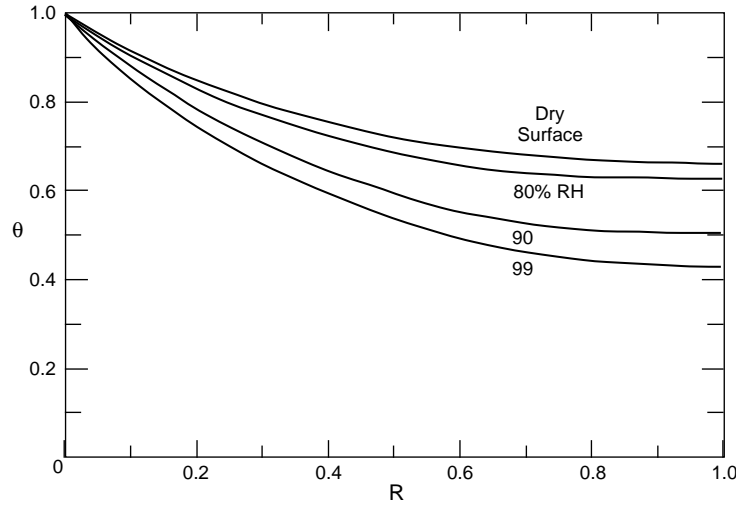
Figure 11. Temperature distributions in a radial fin with moisture condensation from surrounding air. Adapted from Elmahdy and Biggs (1983).

where the constant a (given by eq 54) and c are to be determined from the psychrometric data for the range of temperatures considered. Substituting for $\omega_{T,s}$ from eq 60 into eq 58, the differential equation for T_f becomes

$$\frac{d^2 T_f}{dr^2} + \frac{1}{r}\frac{dT_f}{dr} - \frac{2h}{kw}(T_a - T_f) - \frac{2h_m}{kw}(\omega_a - c - aT_f)h_{fg} = 0. \tag{61}$$

A sample of numerical solution of eq 61 subject to boundary conditions eq 59 is shown in Figure 11. In this figure, the dimensionless temperature $\theta = (T_a - T_f)/(T_a - T_{fb})$ is plotted against dimensionless radius $R = (r - r_b)/(r_t - r_b)$ for dry as well as wet operating conditions. The results are based on the following data: $T_a = 16°C$, $T_{fb} = 7°C$, $h = 57\,W/m^2$ °C, and $N = (r_t - r_b)(2h/kw)^{1/2} = 0.82$. It can be seen that the temperature profiles for a wet fin lie below those of a dry fin. As the relative humidity of air increases, the driving potential for mass transfer increases, which leads to a higher latent heat transfer and higher fin temperature. Note that lower values of θ mean higher fin temperatures

Considering a typical fin surface element $2\pi r dr$, the heat transfer dq to the element can be expressed as

$$dq = \left[h(T_a - T_f) + h_m(\omega_a - \omega_{T,s})h_{fg}\right](2\pi r\, dr). \tag{62}$$

Allowing for heat transfer to both faces of the fin and integrating eq 62, the total heat transfer to the fin is found to be

$$q = \int_{r_b}^{r_t} 4\pi\left[h(T_a - T_f) + h_m(\omega_a - \omega_{T,s})h_{fg}\right]r\, dr . \tag{63}$$

The maximum or ideal heat transfer to the fin occurs if the entire fin surface is maintained at temperature T_{fb}, and is therefore given by

$$q_{ideal} = 2\pi\left(r_t^2 - r_b^2\right)\left[h(T_a - T_{fb}) + h_m(\omega_a - \omega_{b,s})\right] . \tag{64}$$

19

Figure 12. Efficiencies of dry and wet radial fins. Adapted from Elmahdy and Biggs (1983).

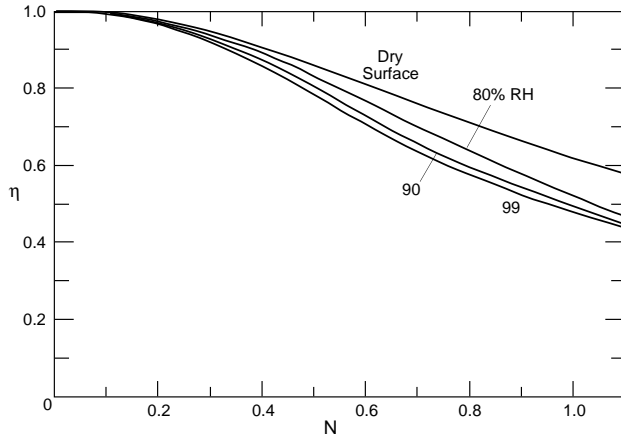The ratio of q/q_{ideal} gives the efficiency of the fin. Figure 12 shows the efficiency as a function of N for both dry and wet fins. This figure is based on the same data as used in Figure 11. The efficiency of a wet fin can be seen as lower than that of a dry fin, and decreases as the relative humidity increases. This can be explained as follows. As the relative humidity increases, the driving potential for mass transfer increases that, in turn, causes q_{ideal} to increase. The corresponding actual q, however, does not increase by the same amount. The net result is a decrease in η.

Conjugate models

This section describes two conjugate models for a cooling and dehumidifying vertical fin of rectangular profile. The first model from Coney et al. (1989a) allows for the coupling between the fin temperature and the condensate film, but assumes the convective heat transfer coefficient to be constant. The approach is essentially the same as in *Simple Models*, except that the model of Coney et al. also includes the effect of mass transfer in writing the energy balance for the fin. The second model described by Kazeminejad et al. (1993) neglects the thermal resistance of the condensate film but allows for the heat transfer coefficient h to vary along the fin. The model finds the variation of h through the solution of boundary layer equations. Both models are discussed in sections that follow.

Coney et al. model

The model considers a vertical rectangular fin as depicted in Figure 13. Taking a slice of fin of volume $bwdz$ and equating the net energy conducted through the slice to the energy convected to the surface $2(b + w)dz$ by simultaneous heat and mass transfer, gives

$$\frac{d^2T_f}{dz^2} = -\frac{2(b+w)q_t''}{kwb} \tag{65}$$

where q_t'' is the total heat flux through the condensate film. Assuming a linear temperature profile for the condensate film, q'' can be expressed as

$$q_t'' = \frac{k_\ell(T_i - T_f)}{\delta} \tag{66}$$

where T_i is the condensate/air interface temperature.

The presence of condensate film can enhance the heat and mass transfer at the condensate-air interface due to increased turbulence and effectiveness roughness. This can be

20
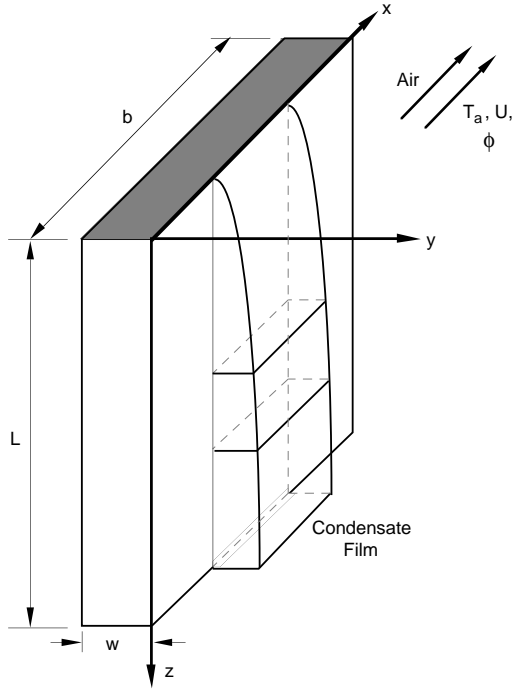
Figure 13. Dehumidification of air on a vertical rectangular fin.

taken into account by multiplying the single-phase heat transfer coefficient h by an interface enhancement factor C_f. C_f depends on geometry and flow conditions, and has to be determined experimentally. Since the minimum value of C_f is unity (for smooth interface at low vapor velocity), the use of $C_f = 1$ would be conservative. The effect of mass transfer on the temperature profile is taken into account by introducing the Ackermann correction factor C_a. Thus, the sensible heat flux, q_s'', between air and condensate film can be expressed as

$$q_s'' = C_f C_a h (T_a - T_i) \ . \tag{67}$$

Eliminating T_i between eq 66 and 67 and denoting the ratio q_s'' / q_t'' by R, the expression for q_t'' becomes

$$q_t'' = \frac{(T_a - T_f)}{\dfrac{\delta}{k_\ell} + \dfrac{R}{C_f C_a h}} \ . \tag{68}$$

Substituting for q_t'' from eq 68 into eq 65, the differential equation governing the temperature distribution in the fin becomes

$$\frac{d^2 T_f}{dz^2} + \frac{2(b+w)}{kwb}\left(\frac{\delta}{k_\ell} + \frac{R}{C_f C_a h}\right)^{-1}(T_a - T_f) = 0 \ . \tag{69}$$

The momentum eq 14 for the condensate film can be adapted for the present analysis as follows:

$$\delta^2 \frac{d\delta}{dz} = \frac{\mu_\ell (1 - R) q_t''}{g \rho_\ell (\rho_\ell - \rho_v) h_{fg}} \ . \tag{70}$$

21

Eliminating q_t'' between eq 68 and 70, the equation governing δ can be written as

$$\delta^2 \frac{d\delta}{dz} - \frac{\mu_\ell(1-R)}{g\rho_\ell(\rho_\ell - \rho_v)h_{fg}} \left(\frac{\delta}{k_\ell} + \frac{R}{C_f C_a h}\right)^{-1} (T_a - T_f) = 0 \ . \tag{71}$$

The simultaneous solution of eq 69 and 71 gives the fin temperature $T_f(z)$ and condensate film thickness $\delta(z)$.

Introducing the following dimensionless variables

$$\left. \begin{aligned} \theta &= (T_a - T_f)/(T_a - T_{fb}), \Delta = \delta/L, \xi = z/L \\[2mm] F_1 &= \frac{g\rho_\ell(\rho_\ell - \rho_v)h_{fg}L^3}{\mu_\ell k_\ell(T_a - T_b)}, F_2 = Bi = \frac{2C_f C_a h L^2 (b+w)}{k_f bw} \\[2mm] F_3 &= \frac{k_\ell}{C_f C_a hL}, F_4 = \frac{1}{F_2 F_3} = \frac{k_f bw}{2k_\ell L(b+w)} \end{aligned} \right\} \tag{72}$$

into eq 69 and 71 gives

$$\frac{d^2\theta}{d\xi^2} = \frac{\theta}{F_4(\Delta + F_3 R)} \tag{73}$$

$$\Delta^2 \frac{d\Delta}{d\xi} = \frac{(1-R)\theta}{F_4(\Delta + F_3 R)} \tag{74}$$

The case of $R = 0$ represents the condensation of pure vapor on a fin, and eq 73 and 74 reduce to eq 16 and 17 of *Simple Models*. Note for a thin fin, $w/b << 1$ and $F_4 = kw/2k_\ell$, which equals F_2 in eq 15. It is also interesting to note that the case of purely convecting fins with no condensation is represented by $R = 1$ and $\Delta = 0$. The range $0 < R < 1$ represents the case of simultaneous heat and mass transfer.

Figure 14 shows typical results for θ obtained from a numerical solution of eq 73 and 74 subject to the boundary condition of constant base temperature ($\xi = 0$, $\theta = 1$) and insulated tip $\xi = 1, d\theta/d\xi = 0$. The parameters F_1, F_2, F_3 and F_4 were calculated assuming moisture condensation on a copper fin (k_f = 380 W/m K) having dimensions of L = 240 mm, b = 220 mm, w = 20 mm. The value of h was calculated using the correlation of Motwani et al. (1985) and assuming the free-stream velocity of U_∞ = 4 m/s, which is typical of air-conditioning systems. Figure 14a illustrates the effect of dry bulb temperature T_a with T_{fb} = 0°C and ϕ = 50%. As T_a increases, θ decreases, indicating an increase in fin temperature T_f. The increase in T_f reflects higher sensible and latent heat transfer to the fin surface. The effect of relative humidity ϕ shown in Figure 14b is similar to that for a radial fin (Fig. 11). Finally, Figure 14c shows that as the fin base temperature T_{fb} is reduced, the driving potential for both heat and mass transfer is increased causing the fin temperature to increase or θ to decrease.

A comparison of dry and wet fin heat transfer is presented in Figure 15. Figure 15a shows the ratio of total heat transfer for wet conditions, q_{wt}, to that for dry conditions, q_d. This ratio decreases with an increase in Biot number. The ratio of sensible heat transfer for wet conditions, q_{ws}, to q_d is plotted in Figure 15b. It can be seen that the sensible heat transfer during condensation is appreciably reduced as Bi increases. Figures 15c,d show
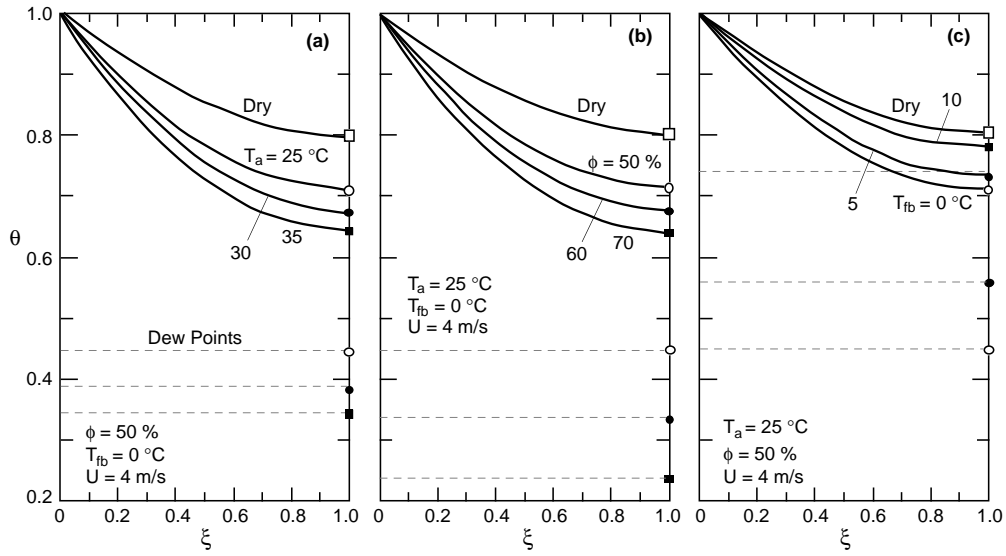
Figure 14. Effects of dry bulb temperature, relative humidity, and fin base temperature on the temperature distributions in a vertical rectangular fin. Adapted from Coney et al. (1989).
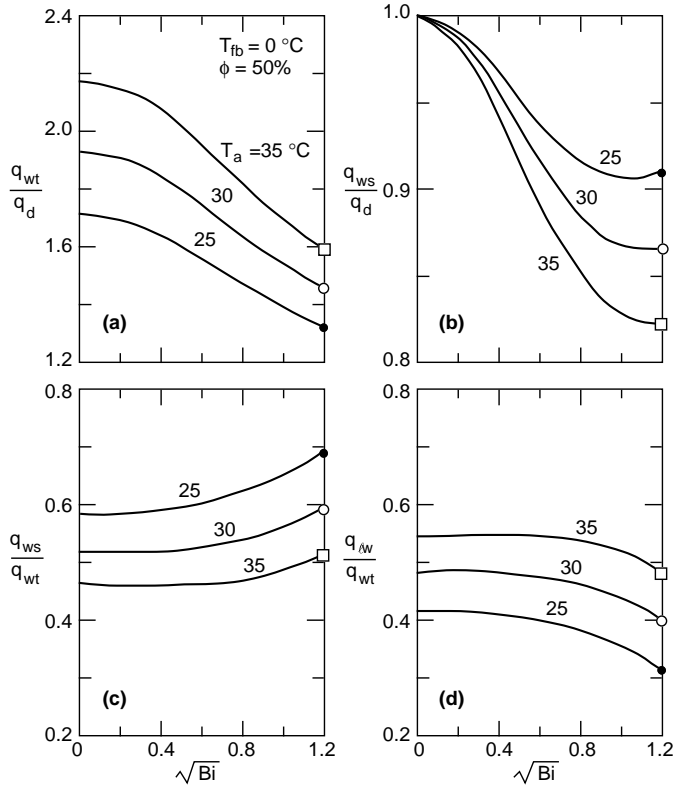
Figure 15. Sensible, latent, and total heat transfers for wet vertical rectangular fins. Adapted from Coney et al. (1989).

how the sensible and latent heat transfers, as a fraction of the total heat transfer for wet conditions, q_{wt}, are affected by Bi and T_a.

The paper by Coney et al. (1989a) also gives the results for the condensate film thickness Δ. These results indicate that Δ increases as T_a and ϕ increase, or as T_{fb} decreases. However, the study concluded that the effect of film thermal resistance can be neglected without introducing significant error for normal conditions encountered in practice. On

23

the other hand, if dropwise condensation occurs, the increased surface roughness and the resultant high turbulence intensity of the fin surface can slightly enhance the heat and mass transfer to the fin.

Kazeminejad et al. model

Kazeminejad et al. (1993) considered a downward pointing vertical fin of rectangular profile (Fig. 4b) with moist air (temperature T_a, relative humidity ϕ) flowing upward with a uniform velocity U_a. They neglected the condensate film thickness Δ in eq 73 but allowed h, appearing in the definition of F_3, to be a function of x, that is $h = h(x)$ where x is measured from the fin tip. To obtain $h(x)$ the nonsimilar boundary layer equations for upward flow over a nonisothermal vertical surface were written as

$$f''' + \frac{1}{2}ff'' = x\left(f'\frac{\partial f}{\partial x} - f''\frac{\partial f}{\partial x}\right) \tag{75}$$

$$\frac{1}{\mathrm{Pr}}g'' + \frac{1}{2}fg' + n(1-g)f' = x\left(f'\frac{\partial g}{\partial x} - g'\frac{\partial f}{\partial x}\right) \tag{76}$$

$$f(x,0) = f'(x,0) = 0, \; f'(x,\infty) = 1; \; g(x,0) = 0, \; g(x,\infty) = 1 \tag{77}$$

where

$$f(\eta) = \psi/(U_a\nu x)^{1/2}, \; \eta = y/(U_a\nu x)^{1/2}$$

$$g = \left[T_f(x) - T(x,\eta)\right]/\left[T_f(x) - T_a\right] \tag{78}$$

$$h = \left(\frac{x}{T_f - T_a}\right)\frac{d(T_f - T_a)}{dx}$$

and primes denote differentiation with respect to η. The local heat transfer coefficient $h(x)$ relates to $g'(0)$ as follows

$$h(x) = k_a\left(\frac{U_\infty}{\nu x}\right)^{1/2}g'(0) . \tag{79}$$

The coupled problem consisting eq 73 with $\Delta = 0$, and the boundary layer equations (75–77) were solved numerically by Kazeminejad et al. (1993) to obtain the fin temperature distribution, total heat transfer to the fin, and the fin efficiency. These results show that the conjugate conduction–boundary layer analysis gives higher fin temperatures and higher fin efficiencies than those predicted by the Coney et al. (1989a) model. This conclusion applies to both dry and wet fins.

Example 4

Air at 25°C and 4 m/s flows over a vertical rectangular fin as shown in Figure 13. The fin that is 240 mm long, 220 mm wide, and 20 mm thick is made of copper (k_f = 380 W/m K). The base of the fin is cooled and maintained at a temperature of 0°C. Assuming that the results of Figures 14 and 15 apply to this fin, calculate the tip temperature and total

heat transferred to the fin for **(i)** perfectly dry air and **(ii)** moist air with a relative humidity of 50 %. Also for moist air, calculate the sensible heat and latent heat contributions to the total heat transfer. Use the following correlations for calculating the average convective heat transfer coefficient h:

$$\frac{hD_h}{k_a} = 0.590 \left(\frac{U_\infty D_h}{\nu_a} \right)^{0.60} \qquad \text{for dry conditions}$$

$$\frac{hD_h}{k_a} = 0.231 \left(\frac{U_\infty D_h}{\nu_a} \right)^{0.69} \qquad \text{for wet conditions}$$

where D_h is the hydraulic diameter and equals $2bL/(b+L)$. These correlations are discussed in the next section.

Solution

The hydraulic diameter D_h is given by

$$D_h = \frac{2bL}{b+L} = 0.23\,\text{m} \;.$$

The thermal conductivity and kinematic viscosity of air at 25°C are $k_a = 0.0255$ W/m K, $\nu_a = 15.5 \times 10^{-6}$ m^2/s.

(i) For dry conditions, the average heat transfer coefficient h is given by

$$h = 47.83 \text{ W/m K.}$$

The Biot number Bi can now be calculated as follows:

$$\text{Bi} = \frac{2hL^2(b+w)}{k_f bw} = 0.79$$

Using Figure 14c to read θ at $\xi = 1$ (fin tip) on the dry fin curve, we get

$$\theta_t = \frac{T_a - T_{ft}}{T_a - T_{fb}} = 0.8$$

or $\qquad T_{ft} = T_a - (0.8)\,(T_a - T_{fb}) = 5°C.$

The efficiency of a dry fin is given by the equation

$$\eta_d = \frac{\tanh (\text{Bi})^{1/2}}{\text{Bi}^{1/2}} = 0.8$$

The ideal heat transfer, q_{ideal}, is given by

$$q_{ideal} = 2h\,(b+w)\,L\,(T_a - T_{fb}) = 137.75 \text{ W} \;.$$

Thus the actual heat transfer q_d is

$$q_d = \eta_d\, q_{ideal} = 110.2 \text{ W.}$$

(ii) For the wet conditions, the average heat transfer coefficient h is given by

$$h = 0.231 \frac{k_a}{D_h} \left(\frac{U_\infty D_h}{\nu_a} \right)^{0.69} = 50.36\,\text{W/m}^2\,\text{K}.$$

The Biot number for the wet conditions is 0.83.

Reading Figure 14c for θ at $\xi = 1$ (fin tip) on the curve for $T_{fb} = 0°\text{C}$, we have

$$\theta_t = \frac{T_a - T_{ft}}{T_a - T_{fb}} = 0.72$$

or $\quad T_{ft} = T_a - 0.72\left(T_a - T_{fb}\right) = 7°\text{C}.$

For $\sqrt{\text{Bi}} = (0.83)^{1/2} = 0.91$, so that Figure 15a for $T_a = 25°\text{C}$ gives

$$\frac{q_{wt}}{q_d} = 1.45$$

or $\quad q_{wt} = 1.45\,q_d = 159.8\,\text{W}.$

Reading the curve for $T_a = 25°\text{C}$ in Figure 15c, the ratio q_{ws}/q_{wt} for $\sqrt{\text{Bi}} = 0.91$ is

$$\frac{q_{ws}}{q_{wt}} = 0.63$$

or $\quad q_{ws} = 100.7\,\text{W}.$

The latent heat transfer is 59.1 W.

Experimental studies

Experimental studies of finned coiled heat exchangers have been carried out by several workers including Bryan (1962), Bettanini (1970), Yoshi et al. (1971) and Guillory and McQuiston (1973). These studies have confirmed that the performance of finned coils is significantly reduced when dehumidification occurs. This reduction is the consequence of lower fin efficiency for wet conditions.

Kazeminejad (1987) and Coney et al. (1989b) conducted an experimental study to investigate the performance of a vertical rectangular fin (Fig. 13) when moist air in turbulent flow dehumidifies on the surface of the fin. The study revealed that the wet fin surface temperature increases with increase in free stream velocity, relative humidity and dry bulb temperature. The increase in wet fin surface temperature also occurs when the fin base temperature is decreased. These observations confirm the theoretical predictions shown in Figure 14. The study also noted that smooth and clean surface copper fins promote dropwise condensation rather than filmwise condensation. Although the effect of mass transfer on the heat transfer coefficient was small, the fin efficiency was markedly reduced under wet conditions. Another interesting conclusion was that the shape of the leading edge of the fin affected the heat and fluid flow. The heat transfer to the fin was higher when the leading edge of the fin was blunt (with attendant flow separation and reattachment) than when the leading edge was elliptical.

Based on their experimental work, Kazeminejad (1987) and Coney et al. (1989b) presented the following correlations for the convective heat transfer coefficient for vertical rectangular fins.

Blunt-edged dry fin:

$$\frac{hD_h}{k_a} = 0.590\left(\frac{U_\infty D_h}{\nu_a}\right)^{0.60} \tag{80}$$

Blunt-edged wet fin:

$$\frac{hD_h}{k_a} = 0.231\left(\frac{U_\infty D_h}{\nu_a}\right)^{0.69}. \tag{81}$$

Elliptical-edged dry fin:

$$\frac{hD_h}{k_a} = 0.420\left(\frac{U_\infty D_h}{\nu_a}\right)^{0.60}. \tag{82}$$

Elliptical-edged wet fin:

$$\frac{hD_h}{k_a} = 0.146\left(\frac{U_\infty D_h}{\nu_a}\right)^{0.69}. \tag{83}$$

Optimum fin design

This section considers the design of optimum dimensioned fins for use in a moist air stream. The discussion will be based on the works of Kilic and Onat (1981) and Toner et al. (1983), and will cover longitudinal fins of rectangular and triangular profiles.

Rectangular fins

Kilic and Onat (1981) considered a vertical rectangular fin as shown in Figure 16a, and modified the classical convecting fin equation to allow for simultaneous heat and mass transfer. The modified equation can be expressed as

$$\frac{d^2T_f}{dx^2} = m^2\left\{(T_f - T_a) - \frac{h_m h_{fg}}{hR_v T_a}\left[P_{va} - P\exp\left(A - \frac{B}{T_f}\right)\right]\right\} \tag{84}$$

where $m = \sqrt{2h/kw}$
   h_m = mass transfer coefficient
   R_v = gas constant for water vapor
   P_{va} = partial pressure of water vapor at temperature T,
   P = total pressure
A and B = constants.

A model similar to eq 84 has also been used by Karniven et al. (1990) to study moisture on fins. The Karniven et al. model allows for radiative heat transfer in addition to convective heat and mass transfer. Furthermore, the model considers a partially wet fin rather than a fully wet fin, and also determines the line separating the wet and dry regions.
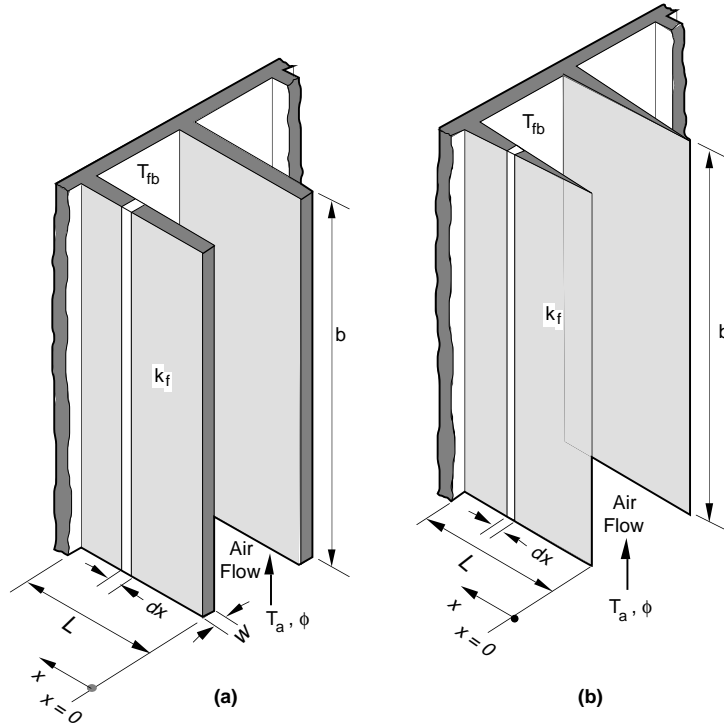
Figure 16. a) Vertical rectangular fins; (b) Vertical triangular fins.

Assuming a constant base temperature and an insulated tip, an approximate analytical solution of eq 84 was derived using the quasi-linearization technique. For a fixed profile area (wL), the expression for heat transfer rate was maximized to yield the following implicit relations for w and L:

$$\frac{w}{L} = m_1 \frac{hL}{k} \tag{85}$$

$$L = \left(\frac{wL k_f}{m_1 h} \right)^{1/3} \tag{86}$$

where

$$m_1 = 1 + \frac{B h_m h_{fg} P_{s,T_r}}{h R_v T_a T_r^2} \tag{87}$$

and

$$T_r = T_a - (T_a - T_{fb}) \frac{\tanh mL}{mL}. \tag{88}$$

Here P_{s,T_r} is the saturation pressure at reference temperature T_r.

A sample solution of eq 85–88 is shown in Figure 17 for atmospheric air with a relative humidity of 50%. The details of evaluation of h_m/h and B can be found in Kilic and Onat (1981). Figure 17 shows that the optimum value of $N = mL$ for a wet fin is lower than that for a dry fin ($N_{opt} = 1.4192$). Also, N_{opt} for a wet fin decreases as the fin base temperature T_b and the free-stream air temperature T_a increase.

28
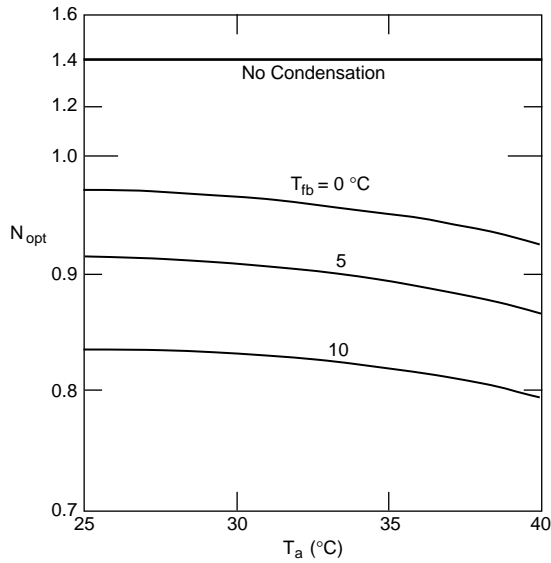
Figure 17. Optimum fin parameter, N_{opt}, for a vertical rectangular fin with moisture condensation. Adapted from Kilic and Onat (1981).
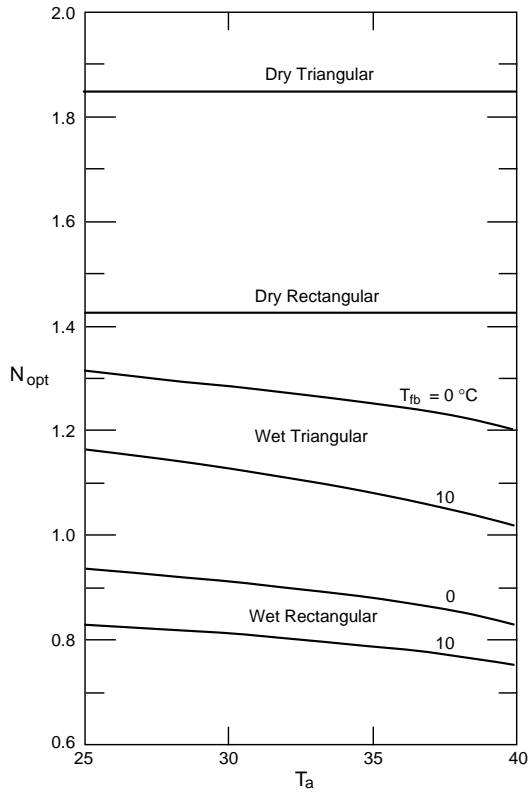
Figure 18. Comparison of N_{opt} for vertical rectangular and vertical triangular fins under dry and wet conditions. Adapted from Toner et al. (1983).

Triangular fins

Toner et al. (1983) extended the analysis of the foregoing section to a vertical fin of triangular profile (Fig. 16b). Figure 18 gives their final results showing how the optimum value of N is affected by the variations of the ambient temperature T_a and fin base temperature T_b. Also shown for comparison are the results for the optimum rectangular fins. It can be seen that for a given T_a and T_b, the optimum value of N for a wet triangular fin is lower than that of a dry triangular fin, and that N_{opt} decreases as T_a and T_b increase. As noted earlier, the wet rectangular fin exhibits the same behavior. It is also interesting to note that the values of N_{opt} for triangular fins (dry and wet) are higher than those of the rectangular fins (dry and wet).

HORIZONTAL INTEGRAL-FIN TUBES

The use of horizontal, low profile integral-fin tubes (Fig. 19) to enhance condensation is quite common in the design of surface condensers in the refrigeration and "process" industries. These tubes have, therefore, been studied extensively for the past fifty years. An excellent review of the pertinent literature has been provided by Marto (1988). The recently published book by Webb (1994) also contains a substantial discussion on the analysis and design of integral-fin tubes.

Commercial integral-fin tubes are made of different materials (aluminum, stainless steel, titanium, copper and its alloys, etc.) and are available in different densities ranging from 433–1675 fins/m or 11–40 fins/in. Although the standard integral-fin design provides a significant enhancement in condensation over plain tubes, more advanced designs such as Hitachi Thermoexcel-C, Wieland GEWA-SC, Wolverine Turbo-C, and Sumitomo Tred-26D improve the performance still further. These designs use a saw-toothed fin shape.

Since the topic of condensation on integral-fin tubes has been comprehensively covered by Marto (1988) and Webb (1994), the following sections will highlight only the important results.
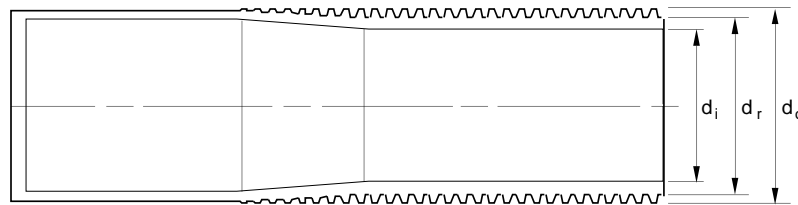
Figure 19. Horizontal integral-fin tube.

Condensate flooding

When a high-surface-tension fluid such as steam condenses on a horizontal finned tube, the surface tension (capillary) force causes the condensate to be retained between the fins on the lower side of the tube as shown in Figure 20a. This phenomenon, which is known as condensate flooding, increases the thermal resistance in the flooded region, thereby adversely affecting the performance of the tube.

Katz et al. (1946) were the first to investigate the phenomenon of liquid retention in horizontal finned tubes. Their measurements, which were performed under static (no condensation) conditions, revealed that in extreme cases, flooding could cover the entire surface of the tube. Rudy and Webb (1981) measured retention of refrigerant R-11, n-pentane, and water in tubes of three different densities (748, 1024 and 1378 fins/m). For the tube with 1024 fins/m, they found that R-11, n-pentane and water flooded 26, 42 and 100 % of the tube circumference, respectively. They also found that flooding under dynamic (condensation) conditions was only slightly different from that under static (no condensation) conditions. The same conclusion was
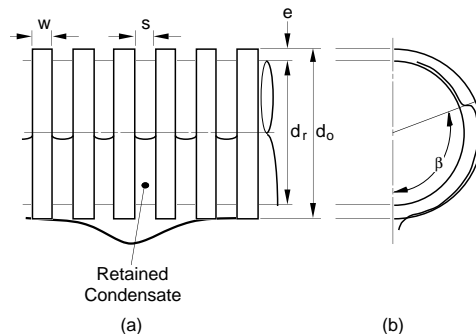
Figure 20. Condensate flooding on a horizontal integral-fin tube.

30
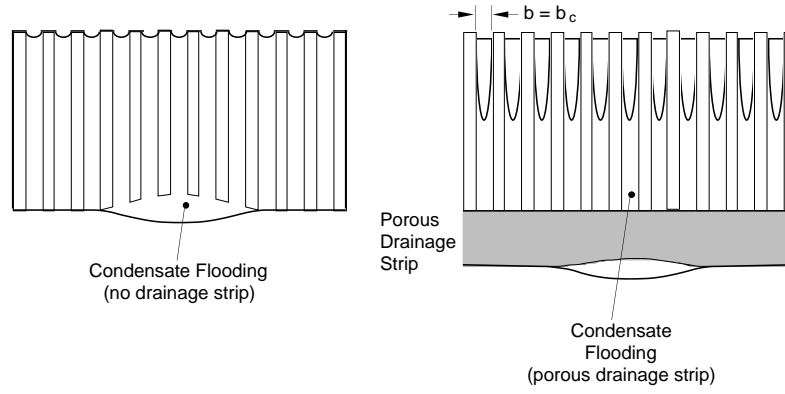
Figure 21. Effect of porous drainage strip on condensate flooding. Adapted from Marto (1988).

reached by Honda et al. (1983) when they found their data for methanol and R-113 under static and dynamic conditions to be essentially the same.

More recent experiments on flooding by Masuda and Rose (1987) have shown that the liquid is not only retained on the lower side of the tube, but also on the upper portion in the form of a small liquid wedge between the flanks of the fins and the tube surface between adjacent fins.

Rudy and Webb (1983a, 1985) and Honda et al. (1983) developed a theoretical expression for the condensate flooding angle *b* (Fig. 20b) by equating the surface tension and gravity forces on the liquid retained between the fins. The expression is

$$\beta = \cos^{-1}\left(1 - \frac{4\sigma}{d_{o}\rho_{\ell}gs}\right) \tag{89}$$

where σ = surface tension
   d_{o} = tube outside diameter
   ρ_{ℓ} = condensate density
   g = acceleration due to gravity
   s = gap between fins.

Equation 89 shows that the flooding angle β increases with increasing surface tension σ and with decreasing fin spacing *s*.

The amount of condensate retained between the fins can be reduced by attaching a rectangular porous plate to the bottom of the tube. This attachment, known as a drainage strip, increases the downward capillary force, drawing the condensate into its pores. Figure 21 illustrates schematically the reduction in condensate flooding achieved with a porous drainage strip. A solid plate can also serve as a drainage strip, but it is not as effective as the porous plate. For example, Honda and Nozu (1987a) measured the effect of different drainage strips for R-113 condensing on an 18.9-mm-diam. (d_{o}) tube having a fin density of 2000 fins/m and a fin height of 1.13 mm. With no drainage strip, they found that 62 % of the tube circumference was flooded. When a polyvinyl chloride strip (solid) of height 12.6 mm was used, the percentage of circumference flooded was reduced to 57, a reduction of about 8 %. However, when a porous nickel strip of the same height (12.6 mm) was attached, only 32 % of the tube circumference was flooded, giving a reduction of about 48 %. Clearly the porous strip is much more effective than a solid strip. The

31

measured heat transfer coefficients for no strip, a PVC strip, and a porous nickel strip were 6200 W/m² K, 6900 W/m² K, and 10,200 W/m² K, respectively. The effectiveness of drainage strips for controlling condensate flooding was also demonstrated by others including Yau et al. (1986) and Marto et al. (1988). Although drainage strips have proved effective under laboratory conditions, their use in an actual condenser tube bundle may not be feasible.

Example 5

Horizontal integral-fin tubes are to be designed to condense steam, ethylene glycol and R-113 at atmospheric conditions.

   (**i**) If the maximum circumference flooded is to be 50 %, calculate the number of fins per meter that should be provided if the outer tube diameter is 19 mm and rectangular fins of 0.25 mm thickness are used.
  (**ii**) If the outer diameter and fin thickness are changed to 21.05 mm and 0.5 mm, respectively, find the new fin density for each of the three fluids.
 (**iii**) Calculate the maximum fin density for steam, ethylene glycol and R-113, condensing on 19-mm outer-diameter tubes, fitted with 0.25-mm-thick rectangular fins.

Solution

   (**i**) For 50 % flooding, $\beta = 90°$ in eq 89. The interfin spacing s is then given by

$$s = \frac{4\sigma}{d_o \rho_\ell g} \ .$$

The values of the ratio σ/ρ_ℓ at atmospheric pressure for the three fluids have been quoted by Marto (1988) as follows:

Steam	$61 \times 10^{-6} \text{ m}^3/\text{s}^2$
Ethylene glycol	$34 \times 10^{-6} \text{ m}^3/\text{s}^2$
R-113	$11 \times 10^{-6} \text{ m}^3/\text{s}^2$.

Thus for steam, the spacing is $s = 1.3$ mm.

The fin density is 645 fins/m.

The above calculations repeated for ethylene glycol and R-113 give fin densities of 1021 and 2057, respectively.

  (**ii**) Repeating the calculations with 21.05-mm-outer diameter and 0.5-mm-thick fins gives densities of 595 fins/m for steam, 863 fins/m for ethylene glycol, and 1402 fins/m for R-113.

 (**iii**) For total flooding, the angle b in eq 89 would be 180°; then the fin spacing s is given by

$$s = \frac{2\sigma}{d_o \rho_\ell g} \ ,$$

which shows the fin spacing is one-half the values obtained in part (a). Thus for steam condensing on 19-mm outer-diameter tube, $s = 0.65$ mm. For a fin thickness of 0.25 mm, the fin density is 1111 fins/m. The corresponding figures for ethylene glycol and R-113 work out to be 1626 and 2717. The value of 1111 fins/m for steam confirms Webb's (1994) statement that condensation of steam on a 19-mm-diam. tube having a 0.25-mm-fin thick-

ness would result in total flooding if the fin density were greater than 1000 fins/m. Indeed, the experimental work of Jaber and Webb (1993) on enhanced tubes for steam condensers shows that integral-fin tubes for steam condensation should use no more than 630 fins/m (16 fins/in.).

Theoretical models for
heat transfer coefficient

Perhaps the first theoretical model for predicting the condensation heat transfer coefficient for integral-fin tubes was proposed by Beatty and Katz (1948). They assumed the condensate flow to be purely gravity driven and applied a Nusselt type analysis for both the fin surface and the tube surface between the fins. The average heat transfer coefficient, $\bar{h}$, for the configuration of Figure 20 was expressed as

$$\bar{h}\eta = h_\text{h}\frac{A_\text{r}}{A} + \eta_\text{f}h_\text{f}\frac{A_\text{f}}{A} \tag{90}$$

where A = heat transfer area
   = $A_\text{r} + A_\text{f}$, A_r
   = surface area of tube at base of fins
   A_f = fin surface area
   η_f = fin efficiency
   η = total surface efficiency
   h_h = heat transfer coefficient for horizontal tube surface
   h_f = heat transfer coefficient for the fin surfaces.

The expressions for h_h and h_f, and the relationship between η and η_f are given by

$$h_\text{h} = 0.728\left[\frac{g\rho_\ell(\rho_\ell - \rho_\text{v})k_\ell^3 h_\text{fg}}{\mu_\ell(T_\text{sat} - T_\text{b})d_\text{r}}\right]^{1/4} \tag{91}$$

$$h_\text{f} = 0.943\left[\frac{g\rho_\ell(\rho_\ell - \rho_\text{v})k_\ell^3 h_\text{fg}}{\mu_\ell(T_\text{sat} - T_\text{b})L_\text{f}}\right]^{1/4} \tag{92}$$

$$\eta = 1 - (1 - \eta_\text{f})\frac{A_\text{f}}{A} \tag{93}$$

where L_f is the average fin height over the diameter d_o equals $\pi(d_\text{o}^2 - d_\text{r}^2)/4d_\text{o}$.

Beatty and Katz (1948) used eq 90 to predict their test data for six low surface tension fluids condensing on finned tubes ranging in fin density from 433 to 630 fins/m. They found that if the coefficient in eq 91 was changed from 0.728 to 0.689, eq 90 predicted their data within 10%. Despite the fact that the Beatty and Katz's model does not account for condensate retention and surface tension effects, the model has enjoyed success in the refrigeration industry for many years.

The first model to include the effect of tension in draining condensate from horizontal finned tubes was presented by Karkhu and Borovkov (1971). They postulated that condensate drainage from the fin surface was purely surface tension driven, while that from the tube surface between the fins was purely gravity driven. From experiments in which R-12 was condensed on the face of a cylinder with machined in rectangular fins, Webb et

al. (1982) concluded that surface tension was indeed the force controlling the condensate drainage from the fin surface. Using a linear surface tension model, Rudy and Webb (1983b) developed the following expression for the heat transfer coefficient on the fin surface:

$$h_{\text{f}} = 0.943 \left[\frac{\rho_\ell k_\ell^3 h_{\text{fg}}}{\mu_\ell (T_{\text{sat}} - T_{\text{b}})} \right]^{1/4} \left[\frac{8\sigma}{(d_{\text{o}} - d_{\text{r}})^2} \left(\frac{1}{w} + \frac{1}{s} \right) \right]^{1/4}. \tag{94}$$

Pursuing the surface tension drainage approach, Adamek (1981) considered a family of convex liquid/vapor interfaces that promote surface tension drainage. The radius of curvature of the family of profiles is described by the equation

$$\frac{1}{r} = \left(\frac{\theta_{\text{m}}}{s_{\text{m}}} \right) \left(\frac{\xi + 1}{\xi} \right) \left[1 - \left(\frac{s}{s_{\text{m}}} \right)^\xi \right] \tag{95}$$

where r = local radius of interface,
    s = distance along the curved interface profile,
    s_{m} = maximum length of the curved interface,
    θ_{m} = rotation angle from tip to fin base
    ξ = interface shape parameter, $-1 \le \xi \le \infty$.

These quantities are illustrated for a typical convex liquid-vapor interface in Figure 22. The relationship between s_{m}, θ_{m}, ξ, and tip radius r_{o} is given by

$$\frac{s_{\text{m}}}{r_{\text{o}} \theta_{\text{m}}} = \frac{\xi + 1}{\xi}. \tag{96}$$

For the condensate profiles described by eq 96, Adamek (1981) obtained the following expression for the condensation heat transfer coefficient:

$$h_{\text{f}} = 2.149 \frac{k_\ell}{s_{\text{m}}} \left[\frac{\rho_\ell \sigma h_{\text{fg}} \theta_{\text{m}} s_{\text{m}}}{\mu_\ell k_\ell (T_{\text{b}} - T_{\text{sat}})} \cdot \frac{\xi + 1}{(\xi + 2)^3} \right]^{1/4}. \tag{97}$$
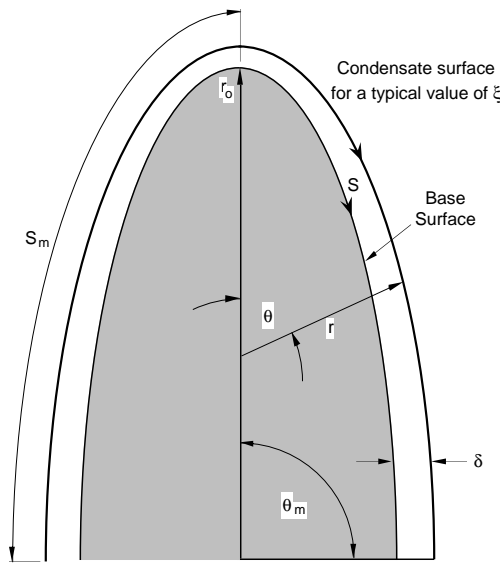

Figure 22. Typical film profile for condensation on a fin with small tip radius, with increasing radius along the arc length.

34

A new family of practical fin profiles for surface tension drained condensation has been described by Kedzierski and Webb (1990). More precise models for surface tension controlled condensation have been developed by Honda and Nozu (1987b), Honda et al. (1987) and Adamek and Webb (1990).

To account for the condensate flooding, Owen et al. (1983) and Webb et al. (1985) suggested that the heat transfer coefficients for the unflooded and flooded parts be computed separately. They recommended that eq 90 should be modified as follows:

$$\bar{h}\eta = \left(1 - \frac{B}{\pi}\right)\left(h_h \frac{A_r}{A} + \eta_f h_f \frac{A_f}{A}\right) + \frac{B}{\pi} h_b \tag{98}$$

where $1 - (B/\pi)$ and B/π represent the fractions of the circumference unflooded and flooded, respectively, and h_b is the heat transfer coefficient for the flooded region. Webb et al. (1985) found that for steam condensing on a 19-mm-diam. tube having 203 fins/m, heat transfer through the flooded region was only 1.6 % of the total. Thus the second term in eq 98 can be neglected for most practical purposes.

In the most recent work, Rose (1994) used some simplifying assumptions, together with dimensional analysis, to develop an equation for calculating the ratio $h_{\text{fined tube}}/h_{\text{plain tube}}$ for condensation on horizontal trapezoidal integral-fin tubes. In a contemporaneous paper, Briggs and Rose (1994) modified the equation given by Rose (1994) to include the effect of fin efficiency.

Example 6

Saturated refrigerant R-12 at 32°C condenses on a horizontal integral-fin tube of outer diameter d_o = 19.1 mm and a root diameter d_r = 15.88 mm. The tube has 748 fins/m. The temperature at the root of the fin is maintained at 22°C. The fins are trapezoidal in shape, 0.38 mm thick at the base and 0.23 mm thick at the tip. Assuming the fin efficiency η_f = 1, calculate the condensation heat transfer coefficient, and the enhancement ratio using 1) the Beatty and Katz (1948) gravity drained model, and 2) the Webb et al. (1985) surface tension drained model. For the surface tension drained model, assume that the condensate film shape is described by the Adamek profile parameters, ξ = –0.857, s_m = 1.5936 mm, and θ_m = 85 degrees (1.4835 radians). The properties of R-12 at the mean film temperature of 27°C (300 K) are

$$
\begin{aligned}
\rho_\ell &= 1305.8 \text{ kg/m}^3 \\
\rho_v &= 40 \text{ kg/m}^3 \\
\nu_\ell &= 19.5 \times 10^{-8} \text{ m}^2/\text{s} \\
k_\ell &= 0.072 \text{ W/m K} \\
\sigma &= 0.0158 \text{ N/m} \\
h_{fg} &= 133.79 \text{ kJ/kg}.
\end{aligned}
$$

Solution

The fin surface per meter of tube length is

$$A_f = 2\frac{\pi}{4}\left(d_o^2 - d_r^2\right)n + \pi d_o w_t n = 0.1458\, \text{m}^2/\text{m}\,.$$

The unfinned surface area of the tube per meter is

$$A_r = \pi d_r - n\pi d_r w_b = 0.0357\, \text{m}^2/\text{m}\,.$$

The total surface of the finned tube per meter is

$$A = A_f + A_r = 0.1815 \ \text{m}^2/\text{m} \, .$$

The heat transfer coefficient for the horizontal (unfinned) surface of the tube is given by eq 91

$$h_h = 0.728 \left[\frac{g(\rho_\ell - \rho_v)k_\ell^3 h_{fg}}{\nu_\ell (T_{sat} - T_b)d_r} \right]^{1/4} = 1540 \ \text{W}/\text{m}^2 \ \text{K} \, .$$

Beatty-Katz model:

The average fin height over the diameter d_o is

$$L_f = \pi \left(d_o^2 - d_r^2 \right) 4 d_o = 0.0046 \ \text{m} \, .$$

The heat transfer coefficient for the fin surface is

$$h_f = 0.943 \left[\frac{g(\rho_\ell - \rho_v)k_\ell^3 h_{fg}}{\nu_\ell (T_{sat} - T_b)L_f} \right]^{1/4} = 2719 \ \text{W}/\text{m}^2 \ \text{K} \, .$$

Because $\eta_f = 1$, $\eta = 1$ from eq 93. Thus the Beatty-Katz model, eq 90 becomes

$$\bar{h} = h_h \frac{A_r}{A} + h_f \frac{A_f}{A} = 2487 \ \text{W}/\text{m}^2 \ \text{K} \, .$$

The enhancement ratio is

$$\frac{\bar{h}}{h_p} = \frac{\bar{h}}{h_h} = 1.63 \, .$$

Based on the envelope area over the fins, $\pi d_o L$, the average heat transfer coefficient is

$$\bar{h} = 7568 \ \text{W} \, \text{m}^2 \ \text{K} \, .$$

Webb et al. model:

For the Adamek condensate film profile, the Webb et al. model uses eq 97 for h_f. Thus

$$h_f = 2.419 \frac{k_\ell}{S_m} \left[\frac{\sigma h_{fg} \theta_m S_m}{\nu_\ell k_\ell (T_{sat} - T_b)} \cdot \frac{\xi + 1}{(\xi + 2)^3} \right]^{1/4} = 4696 \ \text{W}/\text{m}^2 \ \text{K} \, .$$

The average interfin spacing s is calculated by assuming the fin to have an average thickness of $(0.38 + 0.23)/2 = 0.305$ mm. Thus

$$s = 1.032 \ \text{mm} \, .$$

The flooding angle β can now be calculated using eq 89:

$$\beta = \cos^{-1} \left(1 - \frac{4\sigma}{d_o \rho_\ell g s} \right) = 41.44 \ \text{degrees or } 0.72 \ \text{radians} \, .$$

Finally using eq 98 and neglecting the last term, $\bar{h}$ is given by

36

$$\bar{h} = \left(1 - \frac{\beta}{\pi}\right)\left[h_{\mathrm{h}}\,\frac{A_{\mathrm{r}}}{A} + h_{\mathrm{f}}\,\frac{A_{\mathrm{f}}}{A}\right] = 3141\,\mathrm{W/m^2\,K}\,.$$

The enhancement ratio is

$$\frac{\bar{h}}{h_{\mathrm{p}}} = \frac{\bar{h}}{h_{\mathrm{h}}} = 2.04\,.$$

Based on the envelope area over the fins, the average heat transfer coefficient is

$$\bar{h} = \bar{h} = 9501\ \mathrm{W/m^2\ K}\,.$$

The Beatty-Katz model predicts a lower value of $\bar{h}$ than the Webb et al. model. The value of 9501 W/m^2 K is about the same as the value as measured by Webb et al. for condensation of R-11 on 748 fins/m tube (see Fig. 6 in Webb et al. 1985).

Experimental heat transfer coefficients

The review article by Marto (1988) provides a comprehensive listing and discussion of references that report experimental heat transfer data for horizontal finned tubes. Consequently, the brief review here will discuss the difficulties and uncertainties in experimental investigations, present some sample results, and assess the predictive capabilities of the theoretical models in the light of experimental data.

Experimental investigations of film condensation on horizontal integral-fin tubes entail many difficulties. For example, the presence of noncondensable gases, partial dropwise condensation or a substantial vapor velocity near the tube can affect the data significantly, but is rarely brought out in published work. In many cases, the uncertainties in measurements remain obscure. The technique used to determine the average condensation heat transfer coefficient can itself introduce a 10 to 15 % discrepancy between different data. The lack of consistency in the choice of the surface area on which is based often confuses the end user. The interpretation and use of experimental data must therefore be made with great care. The difficulties and uncertainties associated with the measurement of condensation on horizontal integral-fin tubes are discussed in detail by Marto (1992).

Attention is now turned to the discussion of the experimental data. The last fifty years of activity has generated a vast amount of data for condensation of various refrigerants and steam on tubes having different fin geometries and spacing. Only a representative sample can be discussed here. Figure 23 shows the en-
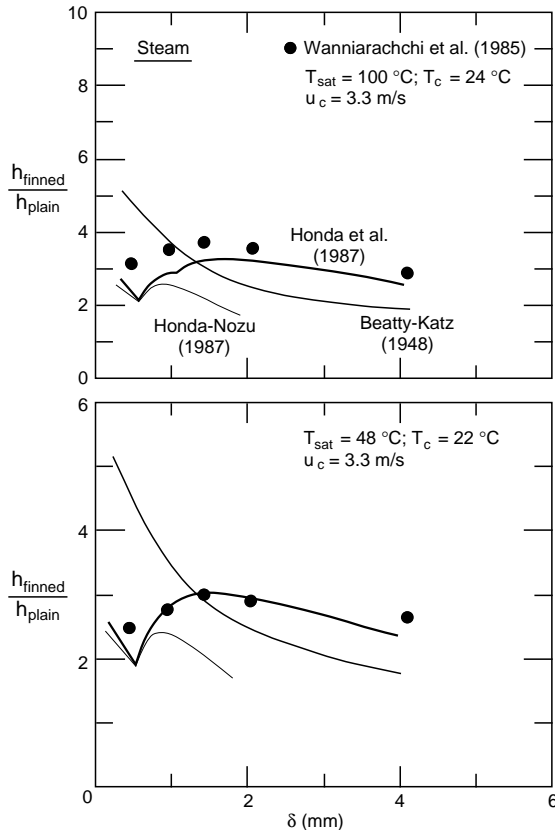

Figure 23. Effect of fin spacing on the enhancement ratio for steam condensing on horizontal integral-fin tubes. Adapted from Honda et al. (1987).
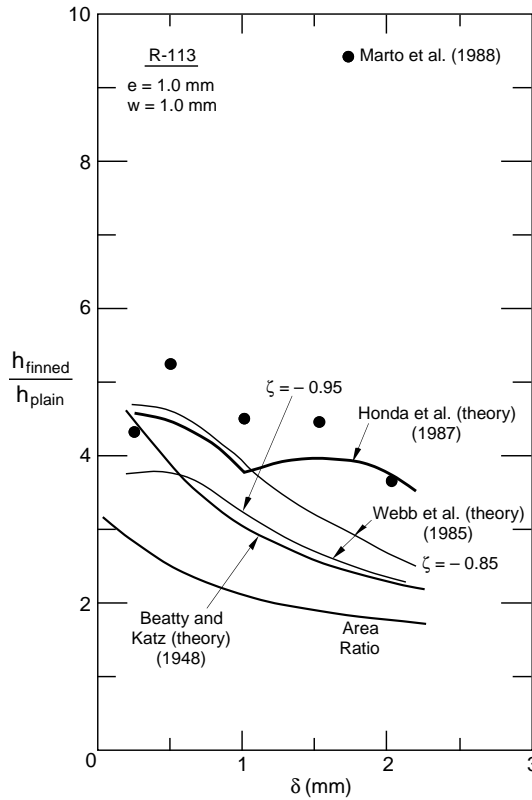
Figure 24. Effect of fin spacing on the enhancement ratio for R-113 condensing on horizontal integral-fin tubes. Adapted from Marto et al. (1988).

hancement ratio $\varepsilon = h_{\text{fined tube}}/h_{\text{plain tube}}$ data of Wanniarachchi et al. (1985) for steam condensing on a family of cooled copper tubes (coolant temperature T_c, coolant velocity U_c) with a root diameter of 19.05 mm and having rectangular integral fins, 1 mm thick and 1 mm high. The figure also shows the predictions of theoretical models of Beatty and Katz (1948), Honda and Nozu (1987b), and Honda et al. (1987). The Beatty-Katz model overpredicts the experimental data at small fin spacings, but underpredicts it at large fin spacings. The Honda-Nozu model underpredicts the data, and the discrepancy gets worse as the fin spacing increases. The predictions of Honda et al. (1987) appear to fit the data best, except at small fin spacings where the flooding is very nearly complete. Although not shown here, the model proposed by Adamek and Webb (1990) predicts the steam data within ±10 to ±15 % over the complete range of fin spacings.

The same family of copper tubes as used by Wanniarachchi et al. (1985) for steam were tested by Marto et al. (1988) for R-113. These results together with the theoretical predictions of Beatty and Katz (1948), Honda et al. (1987) and Webb et al. (1985) are shown in Figure 24. The Beatty-Katz model vastly underpredicts the data. The Webb et al. (1985) theory provides a much better prediction at $\zeta = -0.85$ than at $\zeta = -0.95$. However, the closest agreement with the data is achieved by using the Honda et al. (1987) model.

From the brief discussion here and more extensive coverage elsewhere, e.g., Marto (1988), it appears that virtually all available experimental data pertain to steam and currently popular refrigerants such as R-11, R-12, R-22 and R-113. The data for R-152a, which is a promising alternative to CFCs, are just beginning to appear. Cheng and Tao (1994) are perhaps the first to report experimental work on condensation of R-152a on plain and finned tubes. They conclude that i) the simple Nusselt theory predicts within 15 % the data for condensation on a single smooth tube, ii) the performance of a single smooth tube with R-152a condensing on its outside is 20–25 % better than that obtained with R-12, and iii) the integral fin tube provides enhancement of 4 to 10 times that of a plain tube.

Effect of interfacial shear

It is well known that the interfacial shear stress of the liquid/vapor interface increases the heat transfer coefficient if the vapor and liquid (condensate) flow in the same direction, and decreases it if the two flow in opposite directions. For condensation on plain (smooth) tubes, the effect of vapor velocity has been studied extensively, see for example, Memory and Rose (1986), Honda et al. (1986) and Fujii (1991). However, the correspond-

ing information for the integral-fin tubes is very limited. Webb (1984), Gogonin and Dorokhov (1981) report data for R-12 condensing on two different 800-fins/m tubes, under a range of operating pressure and heat fluxes, and a maximum vapor velocity of 8 m/s. Their data indicate that the effect of vapor velocity for finned tubes is very small compared with the effect for smooth tubes. This observation is in contradiction with the results obtained by Yau et al. (1986), who measured the condensation coefficient for steam condensing on a family of finned tubes and found that the heat transfer enhancement due to assisting vapor shear stress was essentially the same for plain and finned tubes. This latter result has been confirmed in a recent study by Bella et al. (1993) who condensed R-11 and R-113 on a finned horizontal tube, with vapor velocity ranging from 2 to 30 m/s. The work of Bella et al. (1993) concludes that the enhancement due to the vapor velocity begins to appear when the vapor Reynolds number exceeds 10. They also found that the heat transfer coefficient at a vapor velocity of 30 m/s was 50% more than the value for stagnant vapor. Studies by Lee and Rose (1984) and Michael et al. (1989) also underscore the beneficial effect of vapor shear in finned tubes.

Effect of tube bundle geometry

When condensation occurs over a vertical column of tubes, the condensate drains from tube to tube, causing the film thickness to increase on the lower tubes. The net effect is to lower the overall heat transfer coefficient compared with a single tube. The classical Nusselt analysis takes this condensate inundation effect into account by multiplying the single tube heat transfer coefficient by a factor N^{-m} giving

$$\bar{h}_N = \bar{h}_1 N^{-m} \tag{99}$$

when $\bar{h}_N$ = the average heat transfer coefficient for a N-tube column
$\bar{h}_1$ = the average heat transfer for a single tube, given by eq 91
m = an exponent which equals 1/4 for the Nusselt analysis.

The experimental values of $\bar{h}_N$ are usually higher than those predicted by eq 99. The enhancement in $\bar{h}_N$ has been attributed by Fujii (1991) to the splashing of the condensate from one tube as it impinges on the next tube. Kern (1958) recommended $m = 1/6$ to account for the enhancement effect.

Several studies have attempted to apply eq 99 to a column of finned tubes. Katz and Geist (1948) obtained data for R-12, n-butane, and steam condensing on a 6-tube column of finned tubes, each having a fin density of 590 fins/m and 1.6-mm-high fins. They found that eq 99 best fit their data for $m = 0.04$. Marto (1986) also recommends $m = 0.04$ based on his data for a column of integral-fin tubes. Pearson and Withers (1969) used two identical 60-tube condensers to condense R-22. Both condensers were equipped with integral-fin tubes, one having tubes with 748 fins/m and other have tubes with 1024 fins/m. These authors suggested that the average heat transfer coefficient for tube bundles can be estimated by multiplying the Beatty-Katz $\bar{h}_N$, given by eq 90–93, with a correction factor $C_N/N^{1/4}$, where $C_N = 134$ for the 748-fins/m-density tubes and $C_N = 1.31$ for the 1024-fins/m density tubes.

More recently, Webb and Murawski (1990) have conducted experiments on four enhanced tube geometries (1024 standard integral fin, Tred-26D, Turbo C, and GEWA-SC). For each geometry, they arranged five tubes in a column and measured the heat transfer coefficient with R-11 condensing over the column. The data were correlated by an equation of the form

$$\bar{h}_N = a\,\mathrm{Re}_\ell^{-n} \tag{100}$$

where the condensate Reynolds number Re_ℓ equals $4\dot{m}_\ell/\mu_\ell L$. The constants a (W/m^2 K) and n for the four geometries tested together with values of $\bar{h}_N$ for $Re_\ell = 100$ are given below:

> 1024 standard integral fin: $a = 12.90 \times 10^3$, $n = 0$, $\bar{h}_N$ = 12,900 W/m^2 K
> Tred-26D: $a = 269.90 \times 10^3$, $n = 0.576$, $\bar{h}_N$ = 18,956 W/m^2 K
> Turbo C: $a = 257.80 \times 10^3$, $n = 0.507$, $\bar{h}_N$ = 24,885 W/m^2 K
> GEWA-SC = $a = 54.14 \times 10^3$, $n = 0.22$, $\bar{h}_N$ = 19,657 W/m^2 K.

The 1024 standard integral fin exhibits zero row effect ($n = 0$) for the same tube using R-113. The results for $\bar{h}_N$ show that the Turbo C tubes gives the best heat transfer performance. GEWA- SC and Tred-26D tubes perform comparably. The lowest performance is displayed by the 1024 standard integral-fin tubes.

Theoretical models for the effect of tube bundle geometry have been expounded by Ishihara and Palen (1983), El-Meghazy (1986) and Honda et al. (1987).

The combined effects of interfacial shear and tube bundle geometry with integral-fin tubes have been studied for vapor downflow by Smirnov and Lukanov (1972). Their results show that the effect of tube bundle geometry is more pronounced in finned tubes than in plain tubes. The paper by Webb (1984) reviews the work done on the effects of interfacial shear and tube bundle geometry for both plain and integral-fin tubes. The paper recommends that designers of shell-side refrigeration condensers should maintain a certain minimum vapor velocity in all regions of the tube bundle.

Effect of tube thermal conductivity

The bulk of the experiments described in *Experimental Heat Transfer Coefficients* pertain to condensation on copper tubes. Because copper has a high thermal conductivity, the "fin efficiency" effects due to the temperature drop in the fin are small. However, this effect can become more pronounced if tubes of lower thermal conductivity are employed. To determine the effect of thermal conductivity on the performance of horizontal integral-fin tubes, Huang et al. (1994) condensed steam and R-113 on tubes made of copper, brass, and bronze. Each tube had a root diameter of 12.7 mm, with rectangular fins 1 mm thick and spaced 0.5 mm apart. Four tubes of each material were tested with fin heights of 0.5, 0.9, 1.3 and 1.6 mm. For comparison, plain tubes (outside diam. = 12.7 mm) of each material were also tested.

The measured data expressed as the enhancement ratio are given in Table 3. As one might have expected, the effect of lowering the thermal conductivity is to reduce the enhancement ratio. This effect is stronger for steam than for R-113. Consider, for example, the condensation of steam on copper and bronze tubes with 1.6-mm-high fins. The en-

Table 3. Effect of tube material on enhancement ratios, k = 315 W/m K, 112 W/m K, and 78 W/m K for copper, brass and bronze, respectively.

Fin height	Steam			R-113		
(mm)	Copper	Brass	Bronze	Copper	Brass	Bronze
0.5	1.74	1.50	1.50	3.16	3.15	2.96
0.9	1.90	1.63	1.43	4.24	4.35	3.90
1.3	2.05	1.68	1.37	4.60	4.72	4.28
1.6	2.40	1.77	1.39	5.16	5.09	4.91

hancement ratio of 1.39 for a bronze tube is 42 % less than the enhancement ratio of 2.4 for a copper tube. For R-113, the corresponding figure is less than 5 %. The enhancement ratio increases as the fin height increases except for steam condensing on bronze tubes when the trend is opposite. It is also worth noting that the enhancement ratios for R-113 are much higher than those for steam.

INTERNALLY FINNED TUBES

When saturated vapor flows into a cooled tube, vapor condenses on the tube wall forming a condensate film on the tube wall. A variety of flow patterns can arise depending on the mass flux (velocity). For example, when the condensate layer is symmetric and the liquid/vapor interface is sharply defined, the flow is classified as annular flow. Other flow possibilities include bubbly flow, dispersed flow, wavy flow, stratified flow, plug flow, and slug flow. Even for a smooth (plain) tube, the flow is quite complex and difficult to analyze. The presence of internal fins complicates the situation further, and makes it extremely difficult, if not impossible, to develop an accurate physics based model describing the heat and fluid flow processes. Consequently, the discussion in this section, including the pressure drop and heat transfer correlations, will be largely based on experimental studies.

In 1974, two papers, one by Reisbig (1974) and the other by Vrable et al. (1974) reported on the condensation of R-12 in internally finned tubes. Reisbig found the condensation heat transfer coefficient to be 20–40 % greater than the smooth-tube value. However, he did not propose any correlation. Vrable et al. (1974), on the other hand, conducted 26 experiments with two different internally finned tubes, varying the inlet reduced pressure (p/p_{cr}) from 0.18 to 0.46 and the mass flux from 86.7 to 853 kg/m^2 s. The more effective tube was found to give a maximum enhancement of 300 %. The following correlation represented their data within ±30 %:

$$\bar{h} = 0.01 \frac{k_\ell}{d_h}\left(\frac{2d_h G_e}{\mu_\ell}\right)^{0.8} \mathrm{Pr}_\ell^{0.33}\left(\frac{p}{p_{cr}}\right)^{-0.65} \tag{101}$$

where

$$G_\ell = \left[\left(\frac{\rho_\ell}{\rho_v}\right)^{0.5} x + (1-x)\right]G \tag{102}$$

$$
\begin{aligned}
G &= \text{mass flux (velocity)}\\
d_h &= \text{tube hydraulic diameter}\\
x &= \text{vapor quality}\\
p &= \text{pressure}\\
p_{cr} &= \text{critical pressure.}
\end{aligned}
$$

Royal and Bergles (1978) condensed low pressure steam in four internally finned copper tubes, three of which had spiral fins. The geometric data for these fins are given in Table 4. Figures 25 and 26 represent the heat transfer and pressure drop data, respectively. The heat transfer data for finned tubes indicate a significant improvement over the smooth (plain tube). The highest enhancement ratio of 2.3 is achieved with a 15.9-mm outside-diameter tube containing 16 spiraled fins of height 1.45 mm and a helix angle of 3.22 degrees (tube 5). It is also interesting to note that the area ratio (A/Ap) for tubes 3 and 4 is
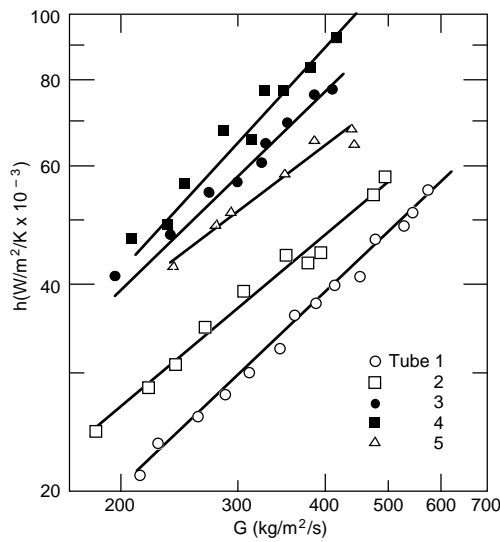
Figure 25. Condensation heat transfer coefficient for condensation of steam in internally finned horizontal tubes. Adapted from Royal and Bergles (1978).
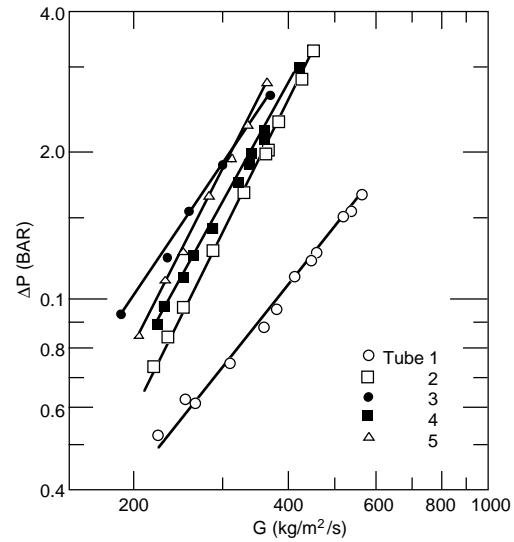
Figure 26. Pressure drop during the condensation of steam in internally finned horizontal tubes. Adapted from Royal and Bergles (1978).

the same, but the heat transfer performance of tube 3 is superior to that of tube 4. Clearly, the area ratio is not the controlling factor. The pressure drop characteristics (Fig. 26) show that the highest pressure drop occurs in tube 3.

Based on their experimental data, they proposed a correlation that represented 95 % of the data within ±30 %. The Royal-Bergles correlation is

$$\bar{h} = 0.0265 \frac{k_\ell}{d_h} \left(\frac{d_h G_\ell}{\mu_\ell} \right)^{0.8} \mathrm{Pr}_\ell^{0.33} \left[160 \left(\frac{e^2}{\bar{s} d_h} \right)^{1.91} + 1 \right] \tag{103}$$

where $\bar{s}$ is the average fin spacing. It is important to note that this correlation was derived for steam at 1.0 bar and may not be accurate for other fluids or pressures. Furthermore, the correlation does not account for the surface tension effects or the temperature gradients in the fin.

Luu and Bergles (1979) tested the tubes of Table 4 with R-113 as the condensing fluid, and found that tube 2, with shortest fins and highest number of fins, exhibited the best heat transfer performance at low flow rates. At high mass flow rates, the measured heat transfer coefficient ranged between 70 and 120 % of the smooth tube value. In a subsequent paper, Luu and Bergles (1980) tested eq 103 against their R-113 data and found it to be unsatisfactory. A new correlation was developed to predict condensation of R-113 in internally finned tubes. However, this correlation overpredicted the data of Said and Azer (1983), who therefore developed their own correlation. In doing so, they excluded the data of Luu and Bergles which was rather unfortunate. Kaushik and Azer (1988) applied regression analysis to the steam data of Royal and Bergles (1978), the

Table 4. Geometric data for internally finned tubes.

Tube no.	d_o (mm)	e (mm)	n	α (°)	A/A_p
1	15.9	—	—	—	1.00
2	15.9	0.60	32	2.95	1.70
3	12.8	1.74	6	5.25	1.44
4	12.8	1.63	6	0	1.44
5	15.9	1.45	16	3.22	1.73

42

R-113 data of Luu and Bergles (1979) and of Said and Azer (1983), and the R-11 data of Venkatesh (1984) to develop a general heat transfer correlation. This correlation was claimed to predict 71% of the data points within ±30%. An analytical model to predict condensation heat transfer in internally finned tubes was proposed by Kaushik and Azer (1989), but the model remains unvalidated against experimental data, and as such can only be recommended with caution.

The information on pressure drop correlation for condensation in internally finned tubes is limited. Kaushik and Azer (1990) used the data of several workers and developed a correlation using the least squares regression technique. This correlation predicted 68 % of the data for steam and R-113 within ±40 %. Sur and Azer (1991) proposed an analytical model, which is claimed to predict the effects of changing the number, height, and thickness of fins on the pressure drop.

So far, the discussion has been focused on condensation of pure vapor. When internally finned tubes are used in the condensers of vapor compression refrigeration systems, the refrigerant vapor is often mixed with small quantities of compressor lubricating oil. This situation has been studied by Schlager et al. (1990a,b) in a two-part paper. In the first part (1990a), the authors reviewed the heat transfer and pressure drop correlations for single-phase and two-phase flows in smooth and internally finned tubes. They found that there was no published correlation for flow of refrigerant-oil mixtures in finned tubes. This conclusion prompted them to embark on an experimental program to study the evaporation and condensation of refrigerant-oil mixtures in smooth and internally finned tubes. The results of this study revealed that the presence of oil lowers the condensation heat transfer coefficient for both smooth and finned tubes. The degradation of heat transfer performance increases as the oil concentration increases. The pressure drop in finned tubes was also found to increase with the increase in oil concentration.

The discussion in this section clearly indicates a need for better understanding of the condensation process in internally finned tubes, so that accurate theoretical models for heat transfer and pressure drop can be developed. There is also a need for correlations, which are more generally applicable and not confined to specific fluids and operating conditions. Similarly, more work is needed to understand and predict condensation of refrigerant-oil mixtures in internally finned tubes.

MICRO-FIN TUBES

The micro-fin tube is currently the most popular enhancement device for residential air-cooled air conditioners (window and central) and automotive refrigerant condensers. This tube geometry was first developed by Hitachi Cable, Ltd., and described in a patent by Fujie et al. (1977). The tube is commercially available in diameters between 4 and 16 mm. The original design, trade named Thermofin, has now been superseded by Thermofin EX, Thermofin HEX, and Thermofin HEX-C. The last design, Thermofin HEX-C, was specially developed for condensation enhancement applications. Figure 27, adapted from
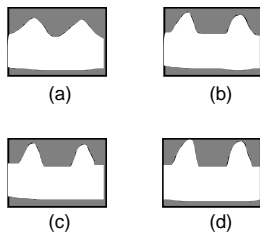
(a) (b)

(c) (d)

Figure 27. Cross sections of Hitachi Thermofin tubes: (a) Thermofin, (b) Thermofin EX; (c) Thermofin HEX; and (d) Thermofin HEX-C. Adapted from Yasuda et al. (1990).

43

Table 5. Characteristics of micro-fin tube designs.

Design	e* (mm)	p/e	α (°)	β (°)	n	A/A$_p$	w$_t$/w$_{tp}$	h/h$_p$
Original	0.15	2.14	25	90	65	1.28	1.22	1.8
EX	0.20	2.32	18	53	60	1.51	1.19	2.4
HEX	0.20	2.32	18	40	60	1.60	1.19	2.5
HEX-C	0.25	2.32	30	40	60	1.73	1.28	3.1

*e = fin height in mm, p = fin pitch, α = helix angle, β = included angle of fin cross-section, n = number of fins in the tube, A = surface area of micro-fin tube, W_t = weight of the tube, h = condensation heat transfer coefficient, and the subscript p denotes the corresponding values for the plain tube.

Yasuda et al. (1990), shows the cross-sections of different micro-fin tubes. Table 5 gives information on geometry, weight, enhancement ratio (for condensation of R-22) for the four micro-fin tube designs (tube outside diameter = 9.52 mm).

The last column of Table 5 shows that the original micro-fin tube improves the condensation coefficient for R-22 by 80% over a plain tube. The subsequent designs, EX and HEX, raise the improvement figure to 140 and 150%, respectively. The HEX-C gives the highest performance with an improvement of 210% over a plain tube. The improved designs have greater fin heights (e) and smaller fin included angles (β). Condensation experiments with micro-fin tubes conducted by Shinohara and Tobe (1985), Shinohara et al. (1987), and Schlager et al. (1990c) have shown that the heat transfer coefficient for R-22 gradually increases with helix angle (α), from 7°, up to 30°. Although these results do not clearly identify the optimum helix angle (α), it does appear that $\alpha = 30°$ results in the best condensation performance.

Figure 28 shows the R-22 condensation heat transfer coefficient as a function of mass flux (velocity) for the tube geometries in Table 5, and demonstrates graphically the superiority of micro-fin tubes over plain tubes. The HEX-C design stands out as distinctly superior to HEX and EX designs for R-22 condensation. The tube outside diameter appears to have little effect on the heat transfer performance.
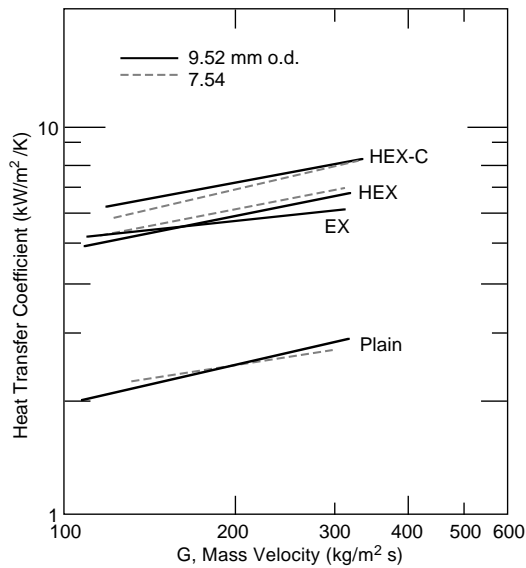

Figure 28. Heat transfer coefficient for R-22 condensing in micro-fin tubes.

44

Pressure drop measurements for R-22 condensing in 12.7-mm-diameter micro-fin tubes have been reported by Schlager et al. (1990c). Their results show that the pressure drop in micro-fin tubes is somewhat higher than that of the plain tube. Because of the uncertainties in the pressure drop measurements, the relative differences between the different microfin tubes could not clearly be established.

The effect of small concentrations of oil in R-22 condensation in micro-fin tubes has been studied by Schlager et al. (1989). The presence of oil generally adversely affects the heat transfer and pressure drop in micro-fin tubes.

Despite the proven effectiveness of the micro-fin tube in practice, detailed work on understanding the enhancement mechanism involved is lacking. Webb (1994) has proposed that both vapor shear and surface tension have important roles to play in augmenting the heat transfer process in micro-fin tubes. There is a great need for experimental work on fluids other than refrigerants so that general purpose correlations for heat transfer and pressure drop in micro-fin tubes can be developed.

CONCLUDING REMARKS

This report described the progress that has been achieved with the analysis and design of extended surfaces for applications involving condensation. The report covered condensation of pure vapor, as well as the condensation of moisture from humid air. The simple models based on Nusselt-type correlations furnish the basic information about the performance of single fins. However, a more detailed picture about the condensate film characteristics and the thermal response of a fin is obtained with conjugate models. Considerable progress has been made in understanding and predicting condensation on horizontal integral-fin tubes. On the other hand, the existing correlations for predicting the performance of internally finned tubes are not only limited in number but also unsatisfactory in many cases. The micro-fin tube, which is currently very popular with condenser designers, remains virtually unexplored both theoretically and experimentally.

The bulk of the information appearing in the literature pertains to analysis. The various analyses have established general guidelines for designing fins for condensation application, but the designer is still left to exercise judgment for designing condensing extended surfaces. This is true of both single fins and an ensemble of fins. Despite 60 years of studies on horizontal integral-fin tubes, these enhanced surfaces are still designed based on past experience. Basic design questions as to the optimum fin shape, size, and number for a specified condensation rate and vapor-tube-coolant combination are still a challenge for researchers. The development of analytical and design tools for the micro-fin tube is still in its infancy.

LITERATURE CITED

Acharya, S., K.G. Braud and A. Attar (1986) Calculation of fin efficiency for condensing fins. *International Journal of Heat and Fluid Flow*, **7**: 96–98.

Adamek, T.A. (1981) Bestimmung der Kondensationgrossen auf Feingewelten oberflachen zur auslegun optimaler Wandprofile. *Warme-und Stoffubertragung*, **15**: 255–270.

Adamek, T.A. and R.L. Webb (1990) Prediction of film condensation on horizontal integral-fin tubes. *International Journal of Heat and Mass Transfer*, **33**: 1721–1735.

Beatty, K.O., Jr. and D.L. Katz (1948) Condensation of vapors on the outside of finned tubes. *Chemical Engineering Progress*, **44**: 908–914.

Bella, B., A. Cavallini, G.A. Longo and L. Rossetto (1994) Pure vapor condensation of refrigerants 11 and 113 on a horizontal integral finned tube at high vapor velocity. *Journal of Enhanced Heat Transfer*, **1**: 77–86.

Bettanini, E. (1970) Simultaneous heat and mass transfer on a vertical surface. *International Institute of Refrigeration Bulletin*, **70**(1): 309–317.

Briggs, A. and J.W.Rose (1994) Effect of fin efficiency on a model for condensation heat transfer on a horizontal, integral-fin tube. *International Journal of Heat and Mass Transfer*, **37**(1): 457–463.

Bryan, W.L. (1962) Heat and mass transfer in dehumdifying extended surface coils. *ASHRAE Journal*, **4**: 60–63.

Burmeister, L.C. (1982) Vertical fin efficiency with film condensation. *ASME Journal of Heat Transfer*, **104**: 391–393.

Cheng, B. and W.Q. Tao (1994) Experimental study of R-152a film condensation on single horizontal smooth tube and enhanced tubes. *ASME Journal of Heat Transfer*, **116**: 266–269.

Coney, J.E.R., H. Kazeminejad and C.G.W. Sheppard (1989a) Dehumidification of air on a vertical rectangular fin: A numerical study. *Proceedings of the Institute of Mechanical Engineers*, **203**: 165–175.

Coney, J.E.R., H. Kazeminejad and C.G.W. Sheppard (1989b) Dehumidification of turbulent air flow over a thick fin: An experimental study. *Proceedings of the Institute of Mechanical Engineers*, **203**: 177–188.

El-Meghazy, I.M. (1986) Enhancing condensation heat transfer on finned tubes in condensers. Ph.D. Thesis (unpublished), Technical University of Warsaw, Poland.

Elmahdy, A.H. and R.C. Biggs (1983) Efficiency of extended surfaces with simultaneous heat and mass transfer. *ASHRAE Transactions*, **89**: 135–143.

Fujie, K., N. Itoh, T. Innami, H. Kimura, N. Nakayama and T. Yanugidi (1977) Heat transfer pipe. U.S. Patent 4,044,797, assigned to Hitachi, Ltd.

Fujii, T. (1991) *Theory of Laminar Film Condensation.* New York: Springer-Verlag, p. 71.

Gogonin, I.I. and A.R. Dorokhov (1981) Enhancement of heat transfer in horizontal shell-and-tube condensers. *Heat Transfer-Soviet Research*, **3**: 119–126.

Guillory, J.L. and F.C. McQuiston (1973) An experimental investigation of air dehumidification in a parallel plate exchanger. *ASHRAE Transactions*, **29**: 146–149.

Honda, H. and S. Nozu (1987a) Effect of drainage strips on the condensation heat transfer performance of horizontal finned tubes. In *Heat Transfer Science and Technology* (B-X. Wang, Ed.). Washington, D.C.: Hemisphere Publishing Corp., p. 455–462.

Honda, H. and S. Nozu (1987b) A prediction method for heat transfer during film condensation on horizontal low integral-fin tubes. *ASME Journal of Heat Transfer*, **109**: 218–225.

Honda, H., S. Nozu and K. Mitsumori (1983) Augmentation of condensation on horizontal finned tubes by attaching a porous drainage plate. *Proceedings of the ASME-JSME Thermal Engineering Joint Conference*, vol. 3, p. 289–296.

Honda, H., S. Nozu and B. Uchima (1987) A generalized prediction method for heat transfer during film condensation on horizontal low finned tube. *Proceedings of the ASME-JSME Thermal Engineering Joint Conference*, vol. 4, p. 385–392.

Honda, H., S. Nozu, B. Uchima and T. Fujii (1986) Effect of vapor velocity on film condensation of R-113 on horizontal tubes in a crossflow. *International Journal of Heat and Mass Transfer*, **29**: 429–438.

Huang, X.S., A. Briggs and J.W. Rose (1994) Effect of thermal conductivity of tube material on condensation heat transfer for integral-fin tubes. In *Proceedings of the 10th International Heat Transfer Conference, Brighton, U.K., August*.

Ishihara, K.I. and J.W. Palen (1983) Condensation of pure fluids on horizontal finned

tube bundles. In *Proceedings of the Symposium on Condensers: Theory and Practice, I.* Chemical Engineering Symposium Series no. 75, p. 429–446.

Jaber, M.H. and R.L. Webb (1993) An experimental investigation of enhanced tubes for steam condensers. *Experimental Heat Transfer*, **6**: 35–54.

Kaarvinen, R., H. Karema and P. Siskanen (1990) Treatment of moisture condensation on fins. *Wärme-und Stoffübertragung*, **25**: 27–31.

Karkhu, V.A. and V.P. Borovkov (1971) Film condensation of vapor at finely-finned horizontal tubes. *Heat Transfer—Soviet Research*, **3**: 183–191.

Katz, D.L. and J.M. Geist (1948) Condensation of six finned tubes in a vertical row. *Transactions ASME*, **70**: 907–914.

Katz, D.L., R.C. Hope and S.C. Datsko (1946) Liquid retention on integral-finned tubes. Department of Engineering Research, University of Michigan, Ann Arbor, Michigan, Project No. M592.

Kaushik, N. and N.Z. Azer (1988) A general heat transfer correlation for condensation inside internally finned tubes. *ASHRAE Transactions*, **94**(2): 261–279.

Kaushik, N. and N.Z. Azer (1989) An analytical heat transfer prediction model for condensation inside longitudinally finned tubes. *ASHRAE Transactions*, **95**(2): 516–523.

Kaushik, N. and N.Z. Azer (1990) A general pressure drop correlation for condensation inside internally finned tubes. *ASHRAE Transactions*, **96**(1): 242–255.

Kazeminejad, H. (1987) Dehumidification of turbulent air flow over a thick fin. Ph.D. Thesis (unpublished), University of Leeds, U.K.

Kazeminejad, H. (1993) Effect of vapor drag on laminar film condensation on a vertical rectangular fin. *Proceedings of the Institute of Mechanical Engineers*, **207**: 63–69.

Kazeminejad, H., M.A. Yaghoubi and F. Bahri (1993) Conjugate forced convection-conduction analysis of the performance of a cooling and dehumidifying vertical rectangular fin. *International Journal of Heat and Mass Transfer*, **36**: 3625–3631.

Kedzierski, M.A. and R.L. Webb (1990) Practical fin shapes for surface-tension-drained condensation. *ASME Journal of Heat Transfer*, **112**: 479–485.

Kern, D.Q. (1958) Mathematical development of loading in horizontal condensers. *AIChE Journal*, **4**: 157–160.

Kern, D.Q. and A.D. Kraus (1972) *Extended Surface Heat Transfer*. New York: McGraw-Hill.

Kilic, A. and K. Onat (1981) The optimum shape for convecting rectangular fins when condensation occurs. *Wärme-und Stoffübertragung*, **15**: 125–133.

Lee, W.C. and J.W. Rose (1984) Forced convection film condensation on a horizontal tube with and without non-condensing gases. *International Journal of Heat and Mass Transfer*, **27**: 519–528.

Lienhard, J.H. and V.K. Dhir (1974) Laminar film condensation on nonisothermal and arbitrary-heat-flux surfaces and on fins. *ASME Journal of Heat Transfer*, **96**: 197–203.

Luu, M. and A.E. Bergles (1979) Experimental study of the augmentation of the in-tube condensation of R-113. *ASHRAE Transactions*, **85**(2): 132–146.

Luu, M. and A.E. Bergles (1980) Enhancement of horizontal in-tube condensation of R-113. *ASHRAE Transactions*, **85**(2): 293–312.

Marto, P.J. (1986) Recent progress in enhancing film condensation on horizontal tubes. In *Proceedings of the 8th International Heat Transfer Conference,* vol. 1, p. 161–170.

Marto, P.J. (1988) An evaluation of film condensation on horizontal integral-fin tubes. *ASME Journal of Heat Transfer*, **110**: 1287–1305.

Marto, P.J. (1992) Film condensation heat transfer measurements on horizontal tubes: Problems and progress. *Experimental Thermal and Fluid Science*, **5**: 556–569.

Marto, P.J., D. Zebrowski, A.S. Wanniarachchi and J.W. Rose (1988) Film condensation

of R-113 on horizontal finned tubes. In *Fundamentals of Phase Change: Boiling and Condensation* (H.R. Jacobs, Ed.), vol. 2, p. 583–592. American Society of Mechanical Engineers.

Masuda, H. and J.W. Rose (1987) Static configuration of liquid films on horizontal tubes with low radial fins: Implications for condensation heat transfer. *Proceedings of the Royal Society of London*, **A410**: 125–139.

McQuiston, F. (1975) Fin efficiency with combined heat and mass transfer. *ASHRAE Transactions*, **81**(1): 350–355.

Memory, S.B. and J.W. Rose (1986) Film condensation of ethylene glycol on a horizontal tube at high vapor velocity. In *Proceedings of the 8th International Heat Transfer Conference* (C.L. Tien et al., Eds.), vol. 4, p. 1607–1612. Washington, D.C.: Hemisphere Publishing Corp.

Michael, A.G., P.J. Marto, A.S. Wanniarachchi and J.W. Rose (1989) Effect of vapor velocity during condensation on horizontal smooth and finned tubes. In *Heat Transfer with Change of Phase, ASME Symposium*, HTD-Vol. 144, p. 1–10.

Motwani, D.G., U.N. Gaitonde and S.P. Sukhatme (1985) Heat transfer from rectangular plates inclined at different angles of attack and yaw to an air flow. *ASME Journal of Heat Transfer*, **107**: 307–312.

Na, T.Y. (1979) *Computational Methods in Engineering Boundary Value Problems*. New York: Academic Press.

Nader, W.K. (1978) Extended surface heat transfer with condensation. Paper CS-5, *Proceedings of the 6th International Heat Transfer Conference*, p. 407–412.

Owen, R.G., R.G. Sardesai, R.A. Smith and W.C. Lee (1983) Gravity controlled condensation on low integral-fin tubes. In *Proceedings of the Symposium on Condensers: Theory and Practice, I.* Chemical Engineering Symposium Series, No. 75, p. 415–428.

Patankar, S.V. and E.M. Sparrow (1979) Condensation on an extended surface. *ASME Journal of Heat Transfer*, **101**: 434–440.

Pearson, J.F. and J.G. Withers (1969) New finned tube configuration improves refrigerant condensing. *ASHRAE Transactions*, **75**: 77–82.

Reisbig, R.L. (1974) Condensing heat transfer augmentation inside splined tubes. *AIAA/ASME Thermophysics Conference, Boston*, Paper 47-HT-7.

Rose, J.W. (1994) An approximate equation for the vapor-side heat transfer coefficient for condensation on low-finned tubes. *International Journal of Heat and Mass Transfer*, **37**: 865–875.

Royal, J.H. and A.E. Bergles (1978) Augmentation of horizontal in-tube condensation by means of twisted tape inserts and internally finned tubes. *ASME Journal of Heat Transfer*, **100**: 17–24.

Rudy, T.M. and R.L. Webb (1981) Condensate retention on horizontal integral-fin tubing. *Advances in Heat Transfer, ASME-HTD*, **18**: 35–41.

Rudy, T.M. and R.L. Webb (1983a) An analytical model to predict condensate retention on horizontal integral-fin tubes. *Proceedings ASME-JSME Thermal Engineering Joint Conference*, vol. 1, p. 373–378. New York: American Society of Mechanical Engineers.

Rudy, T.M. and R.L. Webb (1983b) Theoretical model for condensation on horizontal integral-fin tubes. *Heat Transfer—Seattle 1983, AIChE Symposium Series* (N.M. Farukhi, Ed.), vol. 79, p. 11–18.

Rudy, T.M. and R.L. Webb (1985) An analytical model to predict condensate retention on horizontal integral-fin tubes. *ASME Journal of Heat Transfer*, **107**: 361–368.

Said, S.A. and N.Z. Azer (1983) Heat transfer and pressure drop during condensation inside horizontal finned tubes. *ASHRAE Transactions*, **89**(1): 114–124.

Schlager, L.M., M.B. Pate and A.E. Bergles (1989) Performance of micro-fin tubes with refrigerant-22 and oil mixtures. *ASHRAE Journal*, November, p. 17–28.

Schlager, L.M., M.B. Pate and A.E. Bergles (1990a) Performance predictions of refriger-

ant-oil mixtures in smooth and internally finned tubes—Part I: Literature Review. *ASHRAE Transactions*, **96**(1): 160–169.

Schlager, L.M., M.B. Pate and A.E. Bergles (1990b) Performance predictions of refrigerant-oil mixtures in smooth and internally finned tubes—Part II: Design equations. *ASHRAE Transactions*, **96**(1): 170–182.

Schlager, L.M., M.B. Pate and A.E. Bergles (1990c) Evaporation and condensation heat transfer and pressure drop in horizontal, 12.7 mm micro-fin tubes with refrigerant 22. *ASME Journal of Heat Transfer*, **112**: 1041–1047.

Shinohara, Y. and M. Tobe (1985) Development of an improved Thermofin tube. *Hitachi Cable Review*, No. 4, p. 47–50.

Shinohara, Y., K. Oizumi, Y. Itoh and M. Hori (1987) Heat transfer tubes with grooved inner surface. U.S. Patent 4,658,892, assigned to Hitachi, Ltd.

Smirnov, G.F. and I.I. Lukanov (1972) Study of heat transfer from Freon-11 condensing on a bundle of finned tubes. *Heat Transfer—Soviet Research*, **4**(3): 51–56.

Sur, B. and N.Z. Azer (1991) An analytical pressure drop prediction model for condensation inside longitudinally finned tubes. *ASHRAE Transactions*, **97**(2): 54–61.

Toner, M., A. Kilic and K. Onat (1983). Comparison of rectangular and triangular fins when condensation occurs. *Wärme-und Stoffübertragung*, **17**: 65–72.

Venkatesh, K. (1984) Augmentation of condensation heat transfer of R-11 by internally finned tubes. M.S. Thesis (unpublished), Department of Mechanical Engineering, Kansas State University.

Vrable, D.A., W.J. Yang and J.A. Clark (1974) Condensation of refrigerant-12 inside horizontal tubes with internal axial fins. *Proceedings of the 5th International Heat Transfer Conference*, vol. 3, p. 250–254. New York: Hemisphere Publishing Corporation.

Wanniarachchi, A.S., P.J. Marto and J.W. Rose (1985) Film condensation of steam on horizontal finned tubes: Effect of fin spacing, thickness, and height. *Multiphase Flow and Heat Transfer, ASME HTD*, **47**: 93–99.

Ware, C. and T. Hacha (1960) Heat transfer from humid air to fin and tube extended surface cooling coils. ASME Paper 60-HT-17-1960.

Webb, R.L. (1984) Shell-side condensation in refrigerant condensers. *ASHRAE Transactions*, **90**(1-B): 39–59.

Webb, R.L. (1994) *Principles of Enhanced Heat Transfer*. New York: John Wiley.

Webb, R.L., S.T. Keswani and T.M. Rudy (1982) Investigation of surface tension and gravity effects in film condensation. In *Proceedings of the 7th International Heat Transfer Conference*, vol. 5, p. 175–181. New York: Hemisphere Publishing Corporation.

Webb, R.L., T.M. Rudy and M.A. Kedzierski (1985) Prediction of the condensation coefficient on horizontal integral-fin tubes. *ASME Journal of Heat Transfer*, **107**: 369–376.

Webb, R.L. and C.G. Murawski (1990) Row effect for R-11 condensation on enhanced tubes. *ASME Journal of Heat Transfer*, **112**: 768–776.

Wilkins, J.E., Jr. (1980) Discussion on "Condensation on an extended surface." *ASME Journal of Heat Transfer*, **102**: 186–187.

Yasuda, K., K. Ohizumi, M. Hori and O. Kawamanta (1990) Development of condensing Thermofin HEX-C tube. *Hitachi Cable Review*, No. 9, p. 27–30.

Yau, K.K., J.R. Cooper and J.W. Rose (1986) Horizontal plain and low-finned condenser tubes-effect of fin spacing and drainage strips on heat transfer and condensate retention. *ASME Journal of Heat Transfer*, **108:** 946–950.

Yoshii, T., M. Yamamoto and T. Otake (1971) Effect of dropwise condensation on wet surface heat transfer of air cooling coils. In *Proceedings of the 13th Congress on Refrigeration*, Washington, D.C., p. 285–292.

REPORT DOCUMENTATION PAGE

Form Approved
OMB No. 0704-0188

1. AGENCY USE ONLY (Leave blank)	2. REPORT DATE November 1995	3. REPORT TYPE AND DATES COVERED

4. TITLE AND SUBTITLE
Effect of Condensation on Performance and Design of Extended Surfaces

6. AUTHORS
Virgil J. Lunardini and Abdul Aziz

5. FUNDING NUMBERS

ARO Contract
DAAL03-91-C-0034
TCN 94-077 No. 1140

7. PERFORMING ORGANIZATION NAME(S) AND ADDRESS(ES)

U.S. Army Cold Regions Research and Engineering Laboratory
72 Lyme Road
Hanover, New Hampshire 03755-1290

8. PERFORMING ORGANIZATION REPORT NUMBER

CRREL Report 95-20

9. SPONSORING/MONITORING AGENCY NAME(S) AND ADDRESS(ES)

Army Research Office
Research Triangle Park
Raleigh, North Carolina 27709-2211

10. SPONSORING/MONITORING AGENCY REPORT NUMBER

11. SUPPLEMENTARY NOTES

12a. DISTRIBUTION/AVAILABILITY STATEMENT

Approved for public release; distribution is unlimited.

Available from NTIS, Springfield, Virginia 22161

12b. DISTRIBUTION CODE

13. ABSTRACT (*Maximum 200 words*)

Heat transfer surfaces operating in cold regions often involve condensation. The analytical and experimental progress made in understanding the process of condensation on extended surfaces (fins) is reviewed in detail. The review covers condensation of pure vapor as well as dehumidification of air. The analytical models discussed range from simple Nusselt-type analysis to the three-dimensional conjugate approach, in which the conservation equations for the condensate film are tightly coupled to conduction in the fin. A separate section discusses the topic of dehumidification of air on finned cooling coils. Other topics reviewed include condensation on horizontal integral-fin tubes, convective condensation in internally finned tubes, and condensation in micro-fin tubes. Although condensation on horizontal integral-fin tubes appears to be well understood, our understanding of convective condensation in internally finned tubes, particularly the micro-fin tubes, is very limited. Furthermore, there exists no established methodology for designing extended surfaces for condensation applications. This report contains several examples illustrating the theoretical results that provide some insight into the design process.

14. SUBJECT TERMS		15. NUMBER OF PAGES 59
Condensation Finned surfaces	Heat transfer Refrigeration	16. PRICE CODE

17. SECURITY CLASSIFICATION OF REPORT	18. SECURITY CLASSIFICATION OF THIS PAGE	19. SECURITY CLASSIFICATION OF ABSTRACT	20. LIMITATION OF ABSTRACT
UNCLASSIFIED	UNCLASSIFIED	UNCLASSIFIED	UL